1 **Title**

2 **Stable twin rDNA loci form a single nucleolus in brewer's yeast**

3

4 **Authors**

5 Luciana Lazar-Stefanita[1], Jingchuan Luo[1†], Max A. B. Haase[1,2], Weimin Zhang[1], Jef D.

6 Boeke[1,3]*

7 *, Corresponding author: jef.boeke@nyulangone.org

8 **Affiliations**

9 [1] Institute for Systems Genetics and Department of Biochemistry and Molecular Pharmacology,

10 NYU Langone Health, New York, NY 10016, USA

11 [2] Vilcek Institute of Graduate Biomedical Sciences at NYU School of Medicine

12 [3] Department of Biomedical Engineering, NYU Tandon School of Engineering, Brooklyn NY

13 11201 USA

14 † Present address: Whitehead Institute for Biomedical Research, Cambridge, MA, 02142, USA

15

16 **Keywords**

17 Megablock chromosome engineering, Hi-C genome maps, intra-chromosomal rDNA loci,

18 nucleolar organization, liquid-liquid phase separation.

19

Abstract

The nucleolus is the most prominent membraneless compartment within the nucleus[1,2]. Nucleoli specialize in ribosomal RNA metabolism and are composed of hundreds of ribosomal DNA (rDNA) repeats that form large chromosomal clusters[3–5]. High recombination rates between repeats can cause nucleolar dysfunction correlated to genome instability[6–8], neurodegeneration[9,10] and cell aging[11–13]. Intriguingly, the evolving architecture of genomes has favored a distinct rDNA organization strategy in which a single rDNA locus per chromosome is situated either near the centromere or the telomere[14,15]. To understand how organisms may benefit from these genome configurations, we utilized a fused-karyotype strain of *Saccharomyces cerevisiae*[16] to engineer a chromosome with twin chromosome-collinear rDNA loci. We show that these twin-rDNA strains exhibit neither growth defects nor chromosomal abnormalities, and rapidly adapt to maintain rRNA homeostasis. Using imaging and chromosome conformation capture, we found that the twin loci merge into a single subnuclear compartment throughout the cell cycle. Finally, we showed a direct correlation between locus size and position relative to chromosome landmarks in which the centromere-distal locus undergoes size reduction at a higher frequency compared to the centromere-proximal counterpart. This work uncovers an unexpected feature in the structural evolution of the rDNA while introducing a new model to address cellular metabolism as a function of rDNA dosage.

39 **Introduction**

40 The most abundant genes in cells are those encoding ribosomal RNA (rRNA), usually arranged as
41 a series of tandem repeats that include transcriptional units for rRNAs spaced by non-transcribed
42 sequences[3,17]. As rRNAs are the structural components of ribosomes, they represent the most
43 abundant RNA molecules in most organisms, accounting for 60-70% of cellular transcripts e.g.,
44 10^5/yeast cell[18] and 10^{6-7}/animal cell[1].

45 In eukaryotes, rRNA transcription and ribosome assembly take place in a membraneless organelle
46 that occupies a substantial proportion of the cell nucleus, namely the nucleolus[2,19]. Incongruous
47 features of the nucleolus – such as rapid molecular turnover and liquid-like dynamics, yet
48 maintaining a coherent shape – are reconciled by the liquid-liquid phase separation model[1,20],
49 implying that rRNA and associated proteins self-organize based on intrinsic biophysical
50 properties[21]. Moreover, the structure and activity of the nucleolus are highly dynamic throughout
51 cell division, as is evidently illustrated in eukaryotes with open mitosis in which nucleolar
52 breakdown and transcriptional shutdown are concomitant with entry into mitosis[22,23]. The
53 nucleolus(-i) assembles around distinct chromosomal clusters/loci, gathering hundreds of
54 tandemly repeated rDNA genes that largely exceed the number of units needed for survival.
55 Indeed, typically, only ~50% of the rDNA genes are actively transcribed while the remainder are
56 kept inactive, an equilibrium that can be easily tuned by altering the balance between euchromatin
57 and heterochromatin status at this locus[24,25]. Furthermore, a high rRNA level - positively correlated
58 with growth rate in many microbes[26] - can be achieved not only by boosting transcription but also
59 by rDNA copy number expansion[27]. Given their repetitive nature and the high demand for rRNA
60 transcripts, the rDNA loci are among the most unstable genome structures[7,28]. Their instability
61 relies on a repeat-mediated homologous recombination (HR) mechanism that requires both rDNA

62 replication[27,29] and transcriptional processes[30,31] that often result in clonal size variation in the
63 repeat number.
64 Cyto-taxonomic studies based on the widespread usage of fluorescence in situ hybridization
65 enabled mapping of rDNA loci on chromosomes of thousands of species. Number and position of
66 these loci, each containing hundreds of tandem repeats, were compiled and used for in silico
67 analyses of their evolution in plants[14] and animals[15]. To discover that most taxa have genomes
68 with multiple rDNA loci, with an average number of three to four loci per diploid genome,
69 indicating that most organisms tend to maintain the number of loci moderately low. In plants, locus
70 number was positively correlated with genome size; whereas in animals no such correlation was
71 observed. Surprisingly, although rDNA loci seemed to locate at nearly any chromosomal position,
72 they prevalently appear either pericentromeric and/or peritelomeric (in >75% of karyotypes).
73 Genome-wide studies in mammals[32] and yeasts[33] provided evidence to support the hypothesis that
74 rDNA arrays have changed their chromosomal position multiple times during evolution. Then, in
75 almost every case, the array disappeared entirely from the ancestral site, leaving behind a small
76 'intergenic scar'[33].
77 These insights hint at two potential aspects of rDNA evolution: (*i*) a common ancestral mechanism
78 through which this locus may migrate within genomes and (*ii*) deleterious effects associated with
79 more than a single rDNA locus per chromosome. Regarding the first hypothesis, we can only
80 speculate that HR and 'nonreciprocal crossover' between repeats[34–36] may be responsible for
81 rDNA dynamics. Here we address the second hypothesis by monitoring the effects of rDNA
82 migration event in which the entire megabase rDNA array was transplanted to an ectopic intra-
83 chromosome location through a copy-and-paste mechanism.
84

85 **Results**

86 In budding yeast, such as *Saccharomyces cerevisiae*, the *RDN1* locus is approximately 1.5 Mb
87 region that contains 150 – 200 copies of a 9.1 kb unit and accounts for ~10% of the entire yeast
88 genome[37]. Each repeat encodes for four genes: 5.8S, 25S, 18S and 5S rRNAs transcribed by RNA
89 polymerase I and III[38,39]. The entire array exists in single copy on the right arm of chromosome
90 *12*, located roughly 300 kb from *CEN12* and ~600 kb from *TEL12R* [4,40], and forms a single crescent
91 shaped nucleolus apposed to the nuclear envelope[41] (Figure 1a). To assess whether multiple rDNA
92 loci can support yeast viability, previously constructed strains with a single locus on different
93 chromosomes (chr *12* and chr *3*)[42] were mated and the resulting diploid was sporulated. This
94 allowed the isolation of a haploid strain carrying two rDNA clusters on heterologous
95 chromosomes, validated through pulsed-field gel electrophoresis (PFGE) (Extended Data Figure
96 1a). Notably, this strain displays a single nucleolar compartment (Figure 1b; Extended Data Figure
97 1b). These results led us to conclude that yeast (just like many other eukaryotes) can easily adapt
98 to live with multiple rDNA loci on different chromosomes. However, it leaves unanswered the
99 question of whether the yeast genome can be engineered with multi-megabase rDNA loci
100 coexisting on the same chromosome.

101 *rDNA Megablock engineering: one step transplantation of a megabase locus to a target position*

102 To answer the above question, we used a karyotype-engineered yeast strain carrying three
103 megabase-sized chromosomes (*n*=3; with chromosomes *A*, *B* and *C*) that have been previously
104 generated through sequential telomere fusion events of the sixteen wild-type chromosomes[16].
105 These genome reengineering steps gave rise to megachromosome *C* (5.5 Mb-long), that resulted
106 in a dramatic change in the position of the rDNA locus relative to the nearest active centromere,
107 as illustrated in Figure 1c left cartoon, the black arrowhead points to the rDNA distal position.

108 Precisely stated, on chr *C,* the rDNA-centromere distance increased 9-fold relative to the wild-type
109 distance, reaching up to ~2.7 Mb, whereas its native position relative to the nearest (right arm)
110 telomere remained unchanged. Not only did this 'passive' migration of the locus to a distal location
111 not affect growth (see JL411 strain generated by Luo et al., 2018), but it also provided a
112 chromosomal arm long enough to allow for an insertion of a second centromere-proximal locus in
113 *cis* (Figure 1c right cartoon). Here we developed a variation of the CRISPR-Cas9 editing approach
114 to engineer megachromosomes that we call 'Megablock engineering' (Figure 1c; Methods), in
115 which a megabase-sized segment of a chromosome is moved to a target location, potentially
116 anywhere in the genome. Megablock engineering deploys two CRISPR guide RNAs that cut at the
117 boundaries of the genomic DNA 'block' to be relocated, and a third guide cutting at the target
118 location. Additionally, three 'linker DNAs' are provided: one that joins the native rDNA locus
119 flanking ends together, and two that join the left and right junctions of the target locus to the ends
120 of the megablock (Figure 1c). In this case, the entire megabase long rDNA locus was removed
121 from its native centromere-distal location and relocated 2 Mb closer to the chr *C* centromere. This
122 extremely aggressive genome engineering maneuver was surprisingly efficient, with 6/41 colonies
123 score by PCR genotyping showing evidence of successful megablock engineering, although only
124 one of those simultaneously removed the rDNA from the donor locus and inserted it at the target
125 locus. Hi-C was used to structurally validate the rDNA locus transplantation (Figure 1d, black
126 arrowheads point at the rDNA boundaries). One such strain (JL665), with *CEN* proximal rDNA
127 was then used for further analyses and experiments. Of note, the orientation of the transplanted
128 rDNA array relative to the chromosome was maintained to ensure locus directionality (e.g., rDNA
129 replication and transcription orientation occur centromere-to-telomere in both JL665 and JL411
130 strains with *CEN* proximal or distal rDNA loci, respectively). By mating 'parental' and

131 ‘transplanted’ strains, with either centromere-distal or centromere-proximal rDNA, respectively,
132 we generated a heterozygous diploid with two loci asymmetrically positioned on each homolog of
133 megachromosome *C*. Finally, haploids with duplicated rDNA loci in *cis* were isolated by
134 sporulation of this diploid strain and their integration junctions were PCR-verified (Extended Data
135 Figure 1c, d).

136 *Effects of rDNA duplication on fitness*

137 Whole genome sequencing validated the duplication of the rDNA locus in the haploid strains
138 (LS71 with ‘twin’ rDNA loci) by estimating twice as many rDNA-mapping reads in 2xrDNA/chr
139 *C* (Figure 2a). Importantly, the newly formed rDNA junction sequences were confirmed and no
140 chromosomal abnormalities potentially caused by recombination events between the two collinear
141 loci were detected (Extended Data Figure 2a). Not only did the 2xrDNA isolates lack obvious
142 fitness defects (Figure 2b; Extended Data Figure 2b), but they rapidly adapted to the excess of
143 rDNA repeats by fine-tuning the rRNA levels (Figure 2c; Extended Data Figure 2c). In addition,
144 a small number of genes were differentially expressed in the 2xrDNA vs. 1xrDNA strains (Figure
145 2d; Extended Data Table 2) and represented a nonrandom coherent set of genes. Notably, genes
146 involved in the metabolism of glucose and metal transport were downregulated, whereas phosphate
147 starvation-induced genes were upregulated. These results suggest that twin-rDNA cells may
148 experience a delayed metabolic transition from glucose fermentation (fast-growth) to respiration
149 (slow-growth) in response to nutrient deprivation.

150 Links between function and structure of the rDNA locus in yeast have been previously described,
151 and showed that a subset of the repeats are usually actively transcribed while the remainder are
152 silenced[25,43]. Their transcription level was correlated with distinct chromatin states, defined by the
153 association of the repeats with DNA-folding markers of either euchromatin (e.g., High-mobility

154 group proteins, Hmo1[44]) or heterochromatin (e.g., silencing complex, SIR[45]). Here we identified
155 mild changes in the expression level of these chromatin modifiers: the rDNA-silencing factor
156 (Sir2) was upregulated, whereas the active rDNA copy-associated protein Hmo1 was
157 downregulated in 2xrDNA compared to 1xrDNA strains (Extended Data Figure 2d). This
158 transcriptional anticorrelation is consistent with an excess of repeats in twin-rDNA strains that
159 may demand additional silencing.
160 Next, we investigated the structural organization of chr *C* with twin-rDNA loci in *cis,* and their
161 chromosomal (in)stability.
162 *Structure of chromosomes with twin-rDNA loci in cis*
163 We used Hi-C[46,47] to probe the 3-dimensional (3D) structure of genomes with twin-rDNA arrays.
164 The 2D contact maps of chr *C* containing a single locus, either centromere-proximal or distal, were
165 combined in a single control plot. For comparison purposes, the control plot is displayed adjacent
166 to that obtained from strains with *cis* twin-rDNA loci (Figure 3a). In the control plot, two
167 indistinguishable boundaries formed at each rDNA location, as a result of similar insulation rates
168 from their corresponding adjacent regions. In contrast, the two boundaries in *cis* appeared to give
169 rise to distinct contact frequencies, where the insulation ('sharpness') at the *CEN* proximal rDNA
170 cluster prevailed over the distal twin. This observation was validated through contact
171 quantification plots for each locus that considered contacts between the region enclosed by the two
172 loci and the corresponding non-intervening rDNA-flanking regions (highlighted by blue dashed
173 rectangles in Figure 3a). From this analysis we observed that the distal locus forms a weaker
174 chromosome boundary (lower degree of insulation) when its centromere-proximal twin is located
175 in *cis* (Figure 3b), a result that suggested distinct levels of structural 'bulkiness' between the *cis*
176 rDNA loci.

177 Given that the 2xrDNA map represents consistent results obtained from 3 independent yeast
178 isolates, we reasoned that the structural difference between the twin loci may arise from locus-
179 specific effects. Two major chromatin modifications at the distal locus could potentially be
180 responsible for this difference: (*i*) increased heterochromatin that may result in a highly
181 condensed/compacted structure, and/or (*ii*) a reduction of rDNA repeat copy number. As the two
182 loci are identical in sequence, we were unable to distinguish between rRNA transcripts originating
183 from either locus (see discussion). Even though we may be unable to rule out the hypothesis of
184 different levels of heterochromatin at the two *cis* rDNAs, their overall lengths can be directly
185 measured. The size of each rDNA locus was estimated using PFGE and dual color Southern
186 blotting on BamHI-digested chromosomes (Figure 3c, d; Methods). After digestion with BamHI,
187 which does not cut within the rDNA repeat unit, the rDNA loci were left with unique DNA-
188 flanking sequences, utilized to design probes that specifically recognize each locus. Surprisingly,
189 all 2xrDNA isolates showed a consistent and locus-specific size reduction of the distal rDNA locus
190 of ~500-700 kb when compared to the 1xrDNA-distal parent strain (Figure 3d; Extended Data
191 Figure 3a, b). Also, a higher clonal variability in the size of the distal locus was observed in isolates
192 passaged for ~100 generations (Extended Data Figure 3c). These results led us to hypothesize that
193 rDNA repeats in yeast are more stable when located centromere-proximal rather than distal. To
194 our knowledge this is the first evidence of a direct correlation between size of a repeated region
195 and its relative genome location.
196 Finally, we tested the stability of the two loci in *cis* in function of Sir2, known to suppress
197 recombination between repeated ribosomal genes[30,45]. We found that the two distinct rDNA bands
198 were lost (replaced by DNA smear) in all Δ*sir2* isolates (Extended Data Figure 3d), supporting the
199 idea that the specific size variation of the two loci in *cis* may depend on differential Sir2 activity.

200 *Mitotic reorganization of the nucleolus with cis rDNAs*

201 For the nucleolus to be correctly segregated between mother and daughter cells in late anaphase,
202 rRNA transcription needs to be shut down to achieve rDNA-cluster condensation[48,49]. Importantly,
203 these condensation processes mainly involve the rDNA and are less pronounced across the
204 remainder of the yeast genome.

205 Our previous work showed that the mitotic reorganization of chromatin is preserved along mega-
206 chromosomes (Lazar-Stefanita et al., 2022 in press). Here, we specifically addressed the structure
207 of megachromosome *C* with twin *cis* rDNAs and that of the resulting nucleolus during the cell
208 cycle. Overall we expected chr *C* to undergo a typical mitotic reorganization[50], however it
209 remained unknown how the ~1.9 Mb-long non-rDNA sequence linking the two loci may interfere
210 with the structure of the nucleolus. Cells synchronized in G1 (alpha-factor) and in anaphase
211 (*cdc15-2* ts[51]) were imaged and showed very clearly that the two rDNAs consistently formed a
212 single nucleolar mass per cell throughout mitosis (Figure 4a; Extended Data Figure 4a).

213 Yet the Hi-C maps revealed another layer to the structural complexity of the nucleolus. The G1
214 map displayed strong contacts between the two rDNAs in *cis*, but these were lost in late anaphase
215 (Figure 4b, black arrowhead; Extended Data Figure 4c). Contact quantifications between the
216 rDNA-flanking regions (as described in Figure 3a, b) showed an overall decrease in anaphase
217 compared to G1 (Figure 4b), in agreement with their increase condensation during anaphase that
218 may strengthen chromosome boundaries. Note that the folding status of the rDNA-intervening
219 sequence is not influenced by the rDNA-flanking loci (Extended Data Figure 4b, contact
220 probability $p(s)$ decay). Therefore, we conclude that (*i*) the ~1.9 Mb rDNA-intervening sequence
221 does not interfere with the organization of the nucleolus, and that (*ii*) the two loci are treated as
222 distinct chromosomal entities during anaphase condensation.

Conclusion and discussion

Here we provided the first living evidence of a eukaryotic genome carrying more than one rDNA locus located internally on the same chromosomal arm. The remarkable stability of the yeast genome is highlighted in its transcriptomics and the homeostatic control of the rDNA repeats at each locus. The structure of the twin-rDNA nucleolus and its reorganization during cell cycle was investigated using microscopy and Hi-C, showing a high degree of structural conformity between 1xrDNA and 2xrDNA strains.

Design of the strains

The ectopic location for rDNA-transplantation corresponds to a chromosome fusion site, specifically the right and left ends of chr *15* and chr *4*, respectively. Given that these regions were initially subtelomeric, which typically lack essential genes, we reasoned that they would be 'insensitive-to-insertion' sites for the huge rDNA locus. Finally, the two loci in *cis* conserved the wild-type transcriptional orientation.

Prior works on rDNA have employed interspecies hybrids to address any differential stability of this locus in different yeasts[52–54]. Most of these studies observed a uniparental loss of rDNA genes, a relevant example is the hybrid between *S. cerevisiae* and *S. eubayanus* in which the latter's locus collapsed completely whereas the *S. cerevisiae* remains full sized. Therefore, we reasoned that only by using two native and sequence-identical rDNA arrays located at different positions along the chromosome we could truly evaluate the position-effect on their structure and stability.

Nucleolus as a liquid condensate

245 We found that the rDNA of yeast readily forms a single nucleolus, independent of its: position in
246 the genome (homologous or heterologous chromosomes), number of loci per chromosome (single
247 or duplicated) and repeat size. This is in full agreement with the proposed liquid-liquid phase
248 separation model for the nucleolus[1,21], which envisions the intrinsic biochemical properties of the
249 rDNA as major driving forces for its assembly that can act over very long genomic distances.
250
251 *Potential consequences of a twin-collinear organization of the rDNA loci*
252 Evolutionary analyses of rDNA loci suggested that selective pressure may act to preserve specific
253 characteristics (such as structure, number and position) of these highly repeated loci in eukaryotes.
254 Here we found that placing two rDNA loci in *cis* increases the rate of abnormal meiotic
255 recombination (Extended Data Figure 5), possibly due to mispairing of the homologous
256 chromosomes driven by the rDNA loci. We speculate that the misaligned chromatids can undergo
257 unequal crossing-over resulting in an increased frequency of nonreciprocal exchange of genetic
258 information (or gene conversion) and consequent spore lethality. Our current model suggests that
259 a high meiotic fitness cost is associated with multi-collinear repeated loci, and this would be
260 predicted to ultimately be purged from a sexual population.
261 In addition, the extra copy of the rDNA locus appears to affect the metabolic response to nutrient
262 consumption that would normally induce cells to exit the fast-growing phase, enter slow-growth
263 and eventually arrest. Our transcriptomics data seem to suggests that the rDNA surplus triggers a
264 premature response to starvation congruent with a faster metabolism. Therefore, we speculate that
265 selective pressure acts to maintain rDNA repeats within a so-called 'optimal range' to ensure the
266 most efficient rRNA dosage balance that can be easily tuned in response to environmental changes.
267 More generally, we term this potential fitness defect 'paralogous *cis*-rDNA interference', whereby

268 placement of two repeated and identical sequences in *cis* may cause interference with their
269 function, that would ultimately require the loss of one locus.
270 These findings are noteworthy in the context of rDNA expansions observed in tumor cells, which
271 are usually characterized by genome instability and rapid growth-associated metabolic states
272 predominantly based on fast glucose uptake and fermentation (e.g., the Warburg effect).

273 **Main references**

274 1. Lafontaine, D. L. J., Riback, J. A., Bascetin, R. & Brangwynne, C. P. The nucleolus as a
275 multiphase liquid condensate. *Nat. Rev. Mol. Cell Biol.* **22**, 165–182 (2021).
276 2. Thiry, M. & Lafontaine, D. L. J. Birth of a nucleolus: the evolution of nucleolar
277 compartments. *Trends Cell Biol.* **15**, 194–199 (2005).
278 3. Long, E. O. & Dawid, I. B. Repeated Genes in Eukaryotes. *Annu. Rev. Biochem.* **49**, 727–
279 764 (1980).
280 4. Petes, T. D. Yeast ribosomal DNA genes are located on chromosome XII. *Proc. Natl. Acad.*
281 *Sci. U. S. A.* **76**, 410–414 (1979).
282 5. Sylvester, J. E. *et al.* The human ribosomal RNA genes: structure and organization of the
283 complete repeating unit. *Hum. Genet.* **73**, 193–198 (1986).
284 6. Saka, K., Takahashi, A., Sasaki, M. & Kobayashi, T. More than 10% of yeast genes are
285 related to genome stability and influence cellular senescence via rDNA maintenance. *Nucleic*
286 *Acids Res.* **44**, 4211–4221 (2016).
287 7. Salim, D. & Gerton, J. L. Ribosomal DNA instability and genome adaptability. *Chromosome*
288 *Res.* **27**, 73–87 (2019).
289 8. Weeks, S. E., Metge, B. J. & Samant, R. S. The nucleolus: a central response hub for the
290 stressors that drive cancer progression. *Cell. Mol. Life Sci.* **76**, 4511–4524 (2019).
291 9. Ding, Q., Markesbery, W. R., Cecarini, V. & Keller, J. N. Decreased RNA, and Increased
292 RNA Oxidation, in Ribosomes from Early Alzheimer's Disease. *Neurochem. Res.* **31**, 705–
293 710 (2006).
294 10. Sönmez, A. *et al.* Nucleolar stress controls mutant Huntington toxicity and monitors
295 Huntington's disease progression. *Cell Death Dis.* **12**, 1–12 (2021).

296 11. Ganley, A. R. D. & Kobayashi, T. Ribosomal DNA and cellular senescence: new evidence
297 supporting the connection between rDNA and aging. *FEMS Yeast Res.* **14**, 49–59 (2014).
298 12. Sinclair, D. A., Mills, K. & Guarente, L. Accelerated Aging and Nucleolar Fragmentation in
299 Yeast sgs1 Mutants. *Science* **277**, 1313–1316 (1997).
300 13. Tiku, V. & Antebi, A. Nucleolar Function in Lifespan Regulation. *Trends Cell Biol.* **28**, 662–
301 672 (2018).
302 14. Garcia, S., Kovařík, A., Leitch, A. R. & Garnatje, T. Cytogenetic features of rRNA genes
303 across land plants: analysis of the Plant rDNA database. *Plant J.* **89**, 1020–1030 (2017).
304 15. Sochorová, J., Garcia, S., Gálvez, F., Symonová, R. & Kovařík, A. Evolutionary trends in
305 animal ribosomal DNA loci: introduction to a new online database. *Chromosoma* **127**, 141–
306 150 (2018).
307 16. Luo, J., Sun, X., Cormack, B. P. & Boeke, J. D. Karyotype engineering by chromosome
308 fusion leads to reproductive isolation in yeast. *Nature* **560**, 392–396 (2018).
309 17. Schöfer, C. & Weipoltshammer, K. Nucleolus and chromatin. *Histochem. Cell Biol.* **150**,
310 209–225 (2018).
311 18. Warner, J. R. The economics of ribosome biosynthesis in yeast. *Trends Biochem. Sci.* **24**,
312 437–440 (1999).
313 19. Pederson, T. The Nucleolus. *Cold Spring Harb. Perspect. Biol.* **3**, a000638 (2011).
314 20. Hansen, J. C., Maeshima, K. & Hendzel, M. J. The solid and liquid states of chromatin.
315 *Epigenetics Chromatin* **14**, 50 (2021).
316 21. Feric, M. *et al.* Coexisting Liquid Phases Underlie Nucleolar Subcompartments. *Cell* **165**,
317 1686–1697 (2016).

318 22. Boisvert, F.-M., van Koningsbruggen, S., Navascués, J. & Lamond, A. I. The multifunctional
319 nucleolus. *Nat. Rev. Mol. Cell Biol.* **8**, 574–585 (2007).
320 23. Hernandez-Verdun, D. Assembly and disassembly of the nucleolus during the cell cycle.
321 *Nucl. Austin Tex* **2**, 189–194 (2011).
322 24. Mekhail, K. & Moazed, D. The nuclear envelope in genome organization, expression and
323 stability. *Nat. Rev. Mol. Cell Biol.* **11**, 317–328 (2010).
324 25. Srivastava, R., Srivastava, R. & Ahn, S. H. The Epigenetic Pathways to Ribosomal DNA
325 Silencing. *Microbiol. Mol. Biol. Rev. MMBR* **80**, 545–563 (2016).
326 26. Weider, L. J. *et al.* The Functional Significance of Ribosomal (r)DNA Variation: Impacts on
327 the Evolutionary Ecology of Organisms. *Annu. Rev. Ecol. Evol. Syst.* **36**, 219–242 (2005).
328 27. Kobayashi, T., Heck, D. J., Nomura, M. & Horiuchi, T. Expansion and contraction of
329 ribosomal DNA repeats in Saccharomyces cerevisiae: requirement of replication fork
330 blocking (Fob1) protein and the role of RNA polymerase I. *Genes Dev.* **12**, 3821–3830
331 (1998).
332 28. Kobayashi, T. & Sasaki, M. Ribosomal DNA stability is supported by many 'buffer genes'—
333 introduction to the Yeast rDNA Stability Database. *FEMS Yeast Res.* **17**, fox001 (2017).
334 29. Sanchez, J. C. *et al.* Defective replication initiation results in locus specific chromosome
335 breakage and a ribosomal RNA deficiency in yeast. *PLoS Genet.* **13**, (2017).
336 30. Gottlieb, S. & Esposito, R. E. A new role for a yeast transcriptional silencer gene, SIR2, in
337 regulation of recombination in ribosomal DNA. *Cell* **56**, 771–776 (1989).
338 31. Kobayashi, T. & Ganley, A. R. D. Recombination Regulation by Transcription-Induced
339 Cohesin Dissociation in rDNA Repeats. *Science* **309**, 1581–1584 (2005).

340 32. Robicheau, B. M., Susko, E., Harrigan, A. M. & Snyder, M. Ribosomal RNA Genes
341 Contribute to the Formation of Pseudogenes and Junk DNA in the Human Genome. *Genome*
342 *Biol. Evol.* **9**, 380–397 (2017).
343 33. Proux-Wéra, E., Byrne, K. P. & Wolfe, K. H. Evolutionary Mobility of the Ribosomal DNA
344 Array in Yeasts. *Genome Biol. Evol.* **5**, 525–531 (2013).
345 34. Brown, D. D., Wensink, P. C. & Jordan, E. A comparison of the ribosomal DNA's of
346 Xenopus laevis and Xenopus mulleri: the evolution of tandem genes. *J. Mol. Biol.* **63**, 57–73
347 (1972).
348 35. Eickbush, T. H. & Eickbush, D. G. Finely Orchestrated Movements: Evolution of the
349 Ribosomal RNA Genes. *Genetics* **175**, 477–485 (2007).
350 36. Gibbons, J. G., Branco, A. T., Godinho, S. A., Yu, S. & Lemos, B. Concerted copy number
351 variation balances ribosomal DNA dosage in human and mouse genomes. *Proc. Natl. Acad.*
352 *Sci.* **112**, 2485–2490 (2015).
353 37. Petes, T. D. & Botstein, D. Simple Mendelian inheritance of the reiterated ribosomal DNA of
354 yeast. *Proc. Natl. Acad. Sci.* **74**, 5091–5095 (1977).
355 38. French, S. L., Osheim, Y. N., Cioci, F., Nomura, M. & Beyer, A. L. In Exponentially
356 Growing Saccharomyces cerevisiae Cells, rRNA Synthesis Is Determined by the Summed
357 RNA Polymerase I Loading Rate Rather than by the Number of Active Genes. *Mol. Cell.*
358 *Biol.* **23**, 1558–1568 (2003).
359 39. Nomura, M., Nogi, Y. & Oakes, M. *Transcription of rDNA in the Yeast Saccharomyces*
360 *cerevisiae*. *Madame Curie Bioscience Database [Internet]* (Landes Bioscience, 2013).
361 40. Kim, Y.-H. *et al.* Chromosome XII context is important for rDNA function in yeast. *Nucleic*
362 *Acids Res.* **34**, 2914–2924 (2006).

363 41. Dvorkin, N., Clark, M. W. & Hamkalo, B. A. Ultrastructural localization of nucleic acid
364 sequences in Saccharomyces cerevisiae nucleoli. *Chromosoma* **100**, 519–523 (1991).
365 42. Zhang, W. *et al.* Engineering the ribosomal DNA in a megabase synthetic chromosome.
366 *Science* **355**, (2017).
367 43. Smith, J. S. & Boeke, J. D. An unusual form of transcriptional silencing in yeast ribosomal
368 DNA. *Genes Dev.* **11**, 241–254 (1997).
369 44. Merz, K. *et al.* Actively transcribed rRNA genes in S. cerevisiae are organized in a
370 specialized chromatin associated with the high-mobility group protein Hmo1 and are largely
371 devoid of histone molecules. *Genes Dev.* **22**, 1190–1204 (2008).
372 45. Kobayashi, T., Horiuchi, T., Tongaonkar, P., Vu, L. & Nomura, M. SIR2 regulates
373 recombination between different rDNA repeats, but not recombination within individual
374 rRNA genes in yeast. *Cell* **117**, 441–453 (2004).
375 46. Dekker, J., Rippe, K., Dekker, M. & Kleckner, N. Capturing chromosome conformation.
376 *Science* **295**, 1306–1311 (2002).
377 47. Lieberman-Aiden, E. *et al.* Comprehensive mapping of long-range interactions reveals
378 folding principles of the human genome. *Science* **326**, 289–293 (2009).
379 48. Amon, A. A decade of Cdc14 – a personal perspective. *FEBS J.* **275**, 5774–5784 (2008).
380 49. Clemente-Blanco, A. Nucleolar Condensation: A New Mechanism to Control Mitotic Exit.
381 *Curr. Biol.* **27**, R1220–R1222 (2017).
382 50. Lazar-Stefanita, L. *et al.* Cohesins and condensins orchestrate the 4D dynamics of yeast
383 chromosomes during the cell cycle. *EMBO J.* **36**, 2684–2697 (2017).
384 51. Hartwell, L. H., Culotti, J., Pringle, J. R. & Reid, B. J. Genetic control of the cell division
385 cycle in yeast. *Science* **183**, 46–51 (1974).

386 52. Gordon, J. L. & Wolfe, K. H. Recent allopolyploid origin of Zygosaccharomyces rouxii
387 strain ATCC 42981. *Yeast* **25**, 449–456 (2008).
388 53. Louis, V. L. *et al.* Pichia sorbitophila, an Interspecies Yeast Hybrid, Reveals Early Steps of
389 Genome Resolution After Polyploidization. *G3 Bethesda Md* **2**, 299–311 (2012).
390 54. Nakao, Y. *et al.* Genome sequence of the lager brewing yeast, an interspecies hybrid. *DNA*
391 *Res. Int. J. Rapid Publ. Rep. Genes Genomes* **16**, 115–129 (2009).
392 55. Brachmann, C. B. *et al.* Designer deletion strains derived from Saccharomyces cerevisiae
393 S288C: a useful set of strains and plasmids for PCR-mediated gene disruption and other
394 applications. *Yeast Chichester Engl.* **14**, 115–132 (1998).
395 56. Zavala, A. G., Kulkarni, A. S. & Fortunato, E. A. A Dual Color Southern Blot to Visualize
396 Two Genomes or Genic Regions Simultaneously. *J. Virol. Methods* **198**, 64–68 (2014).
397 57. Truong, D. M. & Boeke, J. D. Resetting the yeast epigenome with human nucleosomes. *Cell*
398 **171**, 1508-1519.e13 (2017).
399 58. Bolger, A. M., Lohse, M. & Usadel, B. Trimmomatic: a flexible trimmer for Illumina
400 sequence data. *Bioinformatics* **30**, 2114–2120 (2014).
401 59. Bray, N. L., Pimentel, H., Melsted, P. & Pachter, L. Near-optimal probabilistic RNA-seq
402 quantification. *Nat. Biotechnol.* **34**, 525–527 (2016).
403 60. Engel, S. R. *et al.* The reference genome sequence of Saccharomyces cerevisiae: then and
404 now. *G3 Bethesda Md* **4**, 389–398 (2014).
405 61. Pimentel, H., Bray, N. L., Puente, S., Melsted, P. & Pachter, L. Differential analysis of RNA-
406 seq incorporating quantification uncertainty. *Nat. Methods* **14**, 687–690 (2017).
407 62. Schneider, C. A., Rasband, W. S. & Eliceiri, K. W. NIH Image to ImageJ: 25 years of image
408 analysis. *Nat. Methods* **9**, 671–675 (2012).

409 63. Langmead, B. & Salzberg, S. L. Fast gapped-read alignment with Bowtie 2. *Nat. Methods* **9**,
410 357–359 (2012).
411 64. Cournac, A., Marie-Nelly, H., Marbouty, M., Koszul, R. & Mozziconacci, J. Normalization
412 of a chromosomal contact map. *BMC Genomics* **13**, 436 (2012).
413

414 **Figures and figure legends**

415 **Figure 1 Transplantation of the rDNA megablock to ectopic genome locations.**

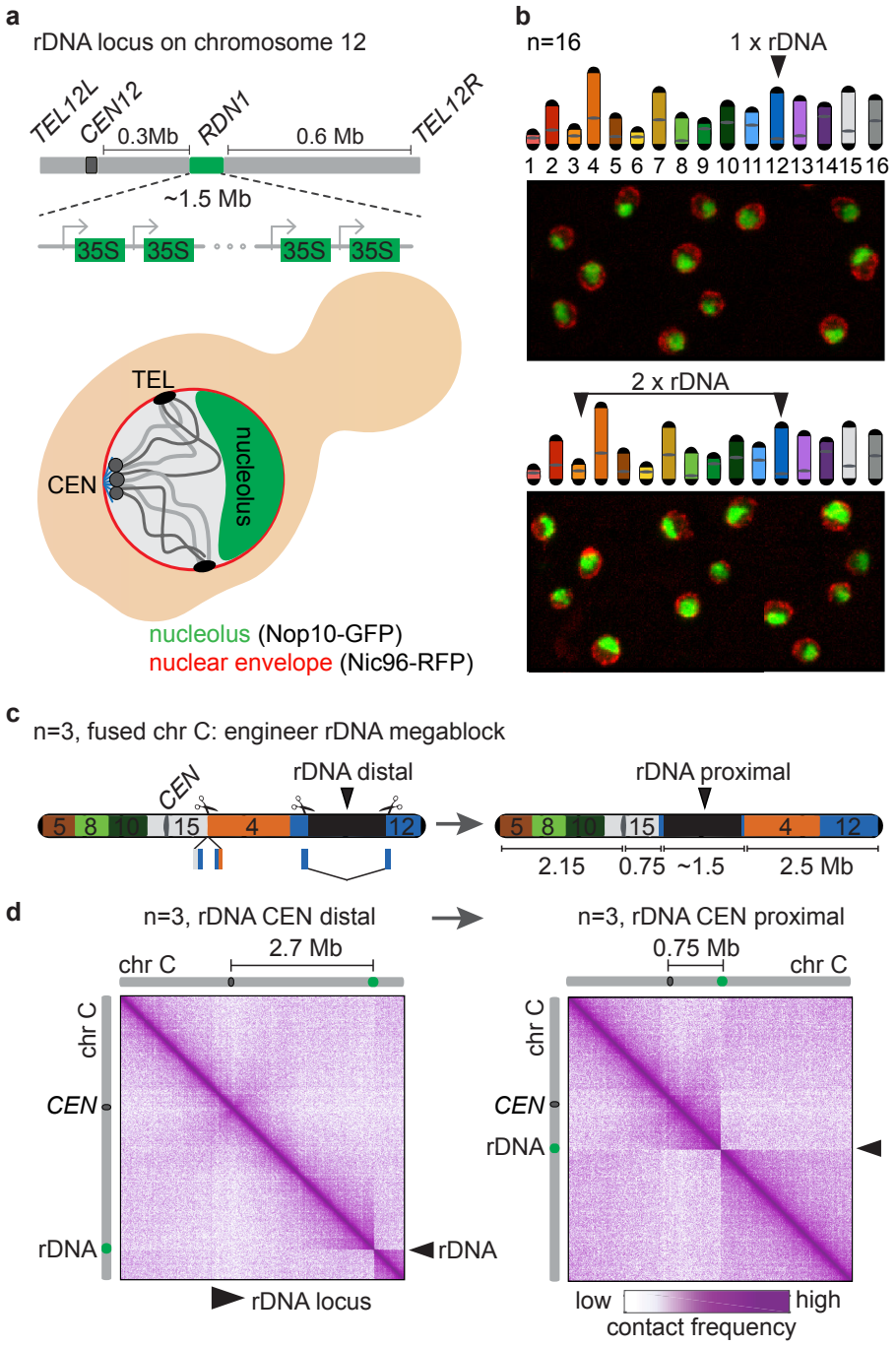

416

417 **Figure 1 Transplantation of the rDNA megablock to ectopic genome locations.**

418 **a** Diagram showing wild-type chromosome *12* that contains the rDNA locus (green) and a
419 simplified representation of nuclear organization in the wild-type yeast, where examples of
420 chromosome arms (gray lines) are anchored at the nuclear membrane through centromeres (*CEN*)
421 and telomeres (*TEL*). **b** Representative microscopy images of yeast nuclei with one or two rDNA
422 loci (black arrowheads indicate rDNA containing chromosomes). **c** Schema illustrating the
423 movement (arrowheads) of the rDNA megablock (black box) on the fused megachromosome *C*
424 (chr *C*: color code corresponds to the design of chromosome fusion) in yeasts with n=3
425 chromosomes. Colored blocks indicate sequence homology of the repair donors at CRISPR-Cas9
426 cutting sites. **d** Hi-C contact maps of chr *C* shown in gray on the *x*- and *y*-axis of each map. The
427 rDNA locus is *CEN* distal on the left, whereas, after transplantation it appears *CEN* proximal on
428 the right. rDNA distance from the centromere (dark gray) is indicated atop the maps.

429

Figure 2 Effects of rDNA duplication on cell fitness.

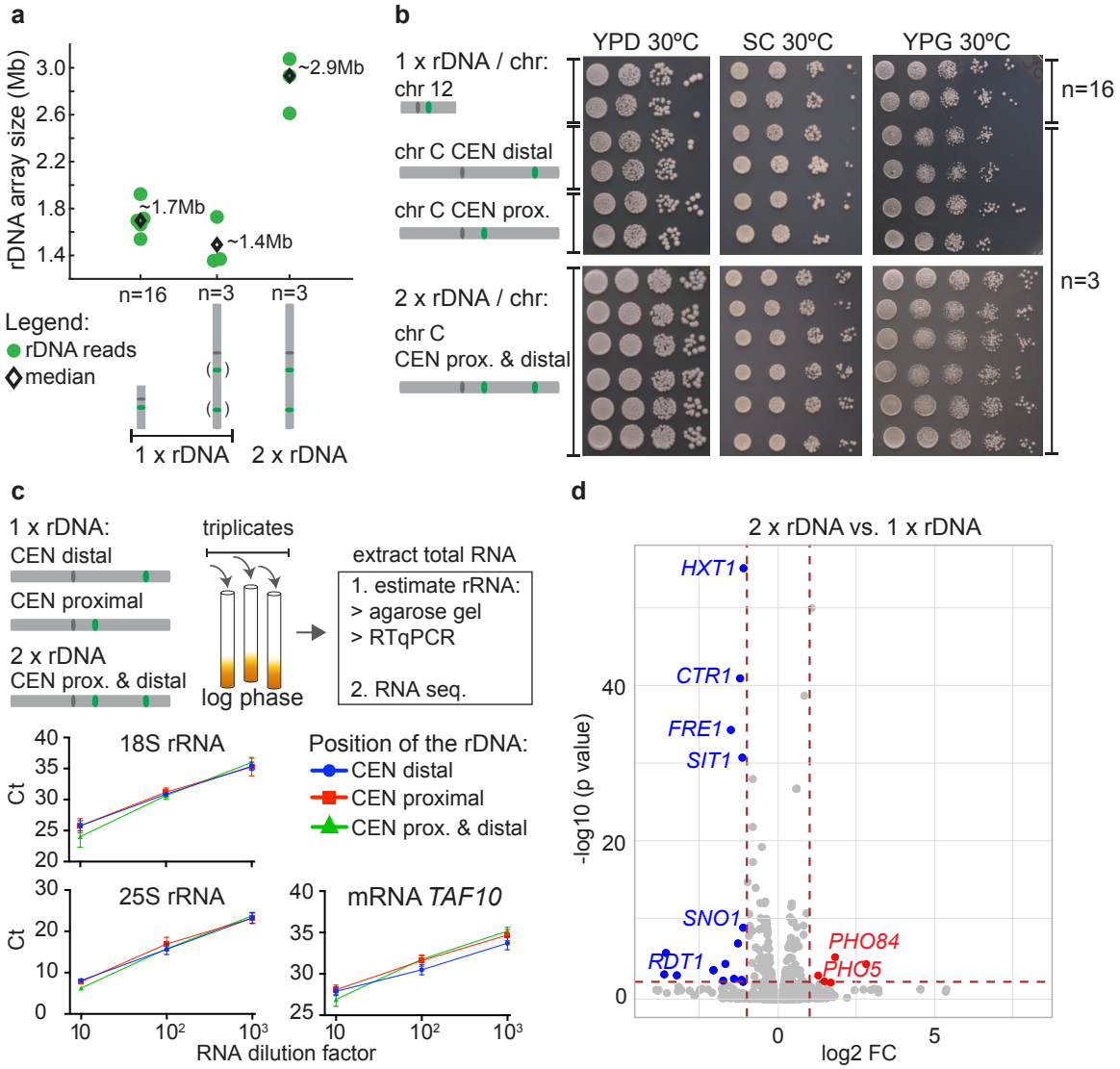

432 **Figure 2 Effects of rDNA duplication on cell fitness.**

433 **a** Estimate the size of the rDNA array in triplicates using deep sequencing (ratio: rDNA aligned
434 reads / total reads). Megachromosome *C* schematics are shown on the bottom of the plot (gray),
435 where round brackets indicate either the proximal or the distal rDNA locus (green). **b** Serial
436 dilution assay on different growing conditions at 30ºC of n=16 and n=3 isolates with either single
437 or duplicated rDNA. **c** Schematics of RNA-based assays in n=3 isolates with 1xrDNA vs 2xrDNA.
438 RTqPCR plots on three serial (1:10) dilutions of total RNA are used to estimate changes in the
439 amount of 18S and 25S ribosomal RNAs relative to the control messenger RNA, *TAF10*. **d**
440 Volcano plot showing RNA-seq data comparing transcriptomes of 1xrDNA and 2xrDNA strains
441 in triplicates. Red and blue dots indicate differentially expressed genes in 2xrDNA vs. 1xrDNA:
442 in blue downregulated in red upregulated ($P < 10-5$, |fold change| > 2).

443

Figure 3 Stability of the rDNA locus is a function of chromosome position.

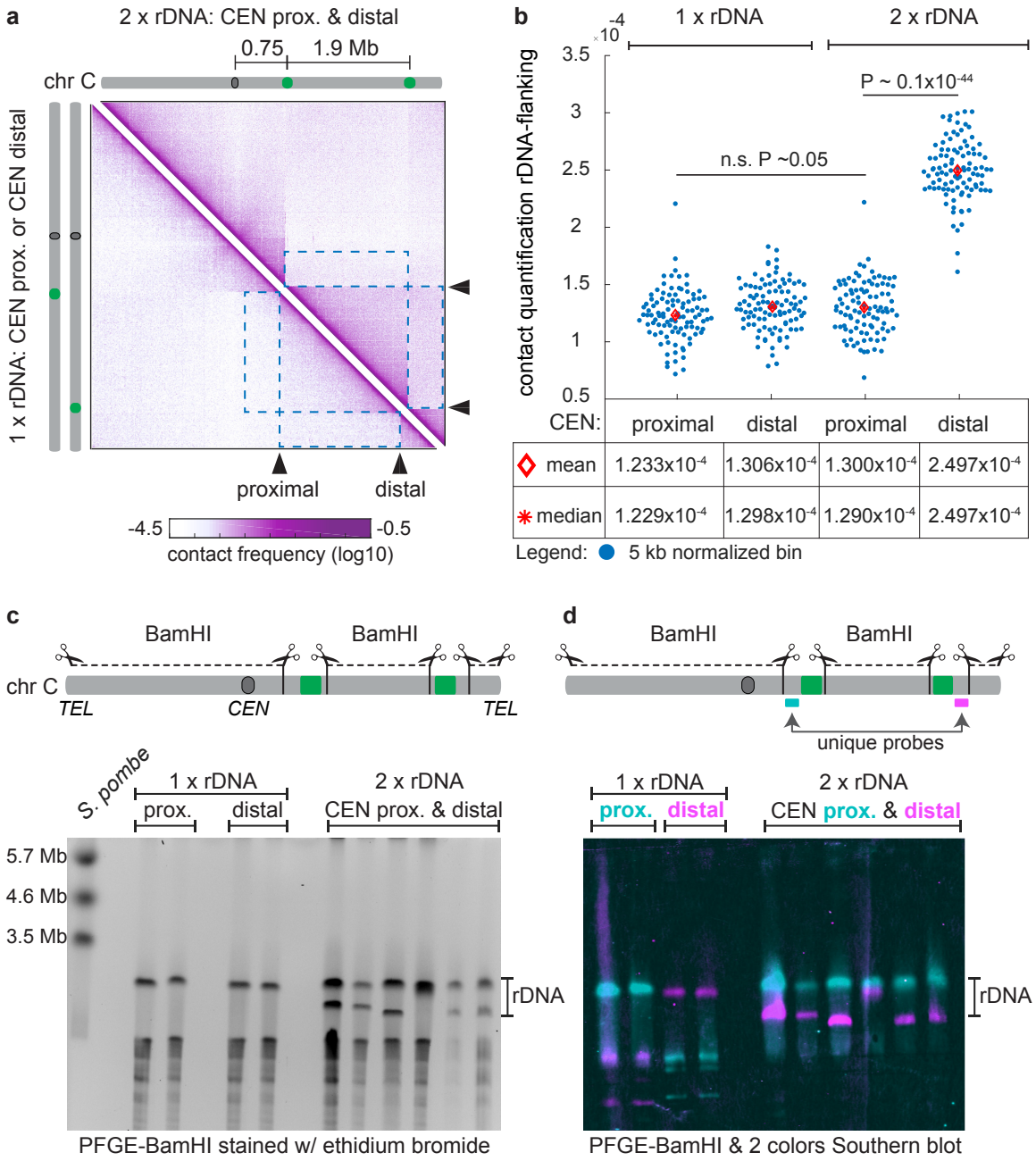

447 **Figure 3 Stability of the rDNA locus is a function of chromosome position.**

448 **a** Hi-C contact maps of megachromsome *C* (chr *C* in gray on the *x*- and *y*-axis of each contact
449 map) in *n*=3 strains with either one or two rDNA loci. Bottom left triangle map: average
450 representation of two merged contact maps with 1xrDNA per chr *C*, either *CEN* proximal or *CEN*
451 distal. Top right map: average representation of three merged contact maps with 2xrDNA per chr
452 *C*, *CEN* proximal and distal. rDNA distance from the centromere (dark gray) is indicated atop the
453 map. **b** Contact quantification between rDNA-flanking regions on chr *C*, highlighted in blue
454 rectangles in panel (a): 500 kb sequence, either upstream *CEN* proximal or downstream *CEN*
455 distal, and the 1.9 Mb sequence, downstream or upstream, respectively. Mean, median of absolute
456 contact values and their *P* values are indicated for each strain with either one or two rDNA loci. **c**
457 - **d** Estimate size of the rDNA arrays. PFGE of BamHI digested chromosomes (c) and the
458 corresponding southern blot (d) with unique probes designed for each rDNA position. PFGE run
459 specifications: *S. pombe* program for mega-size chromosome separation.

460

461 **Figure 4 Twin rDNA loci in *cis* form a single nucleolus during cell division.**

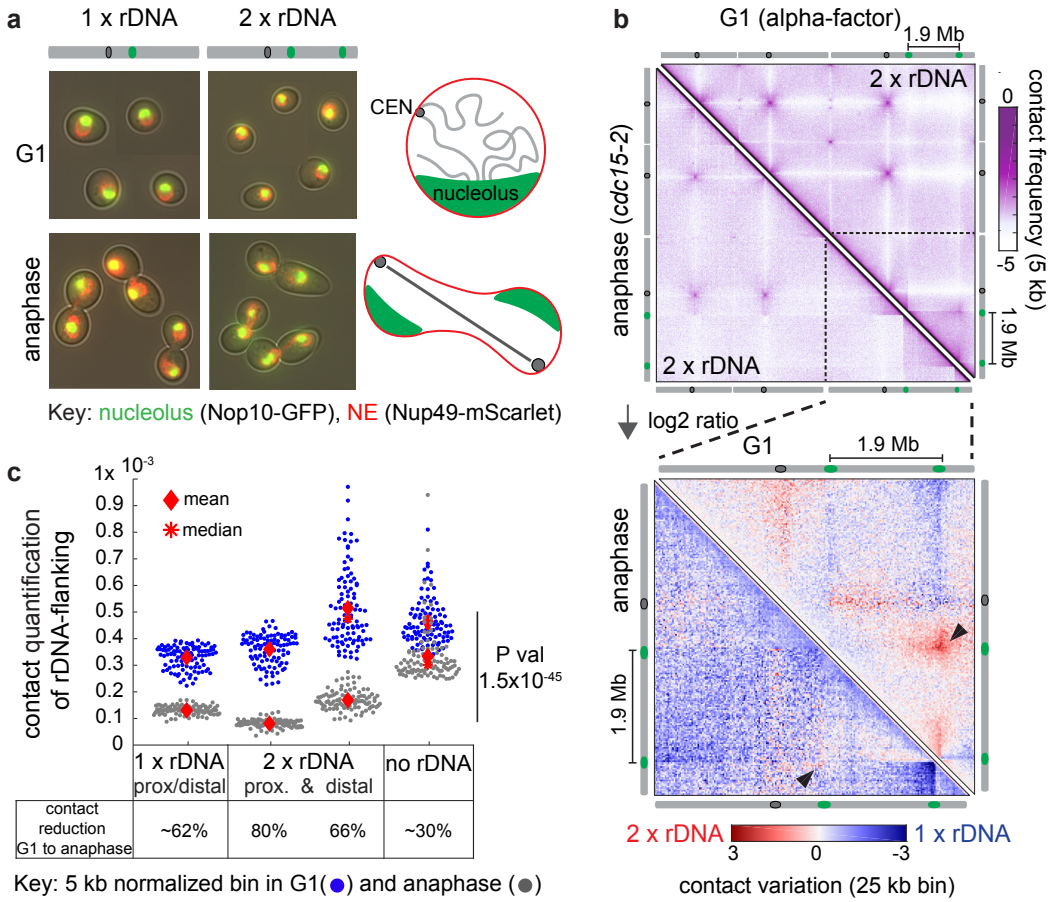

462

463

464 **Figure 4 Twin rDNA loci in *cis* form a single nucleolus during cell division.**

465 **a** Representative microscopy images of *n*=3 cells with one or two rDNA loci in *cis*. Cells were
466 synchronized in G1 (alpha-factor) and late anaphase (*cdc15-2* ts) before imaging. **b** Top panel: Hi-
467 C maps of megachromsomes in *n*=3, with two rDNA loci in *cis* on chr *C* (dashed outline), from
468 cells synchronized in G1 (top right map) and late anaphase (bottom left map). Bottom panel:
469 contact variation maps (log2-ratio) of chr *C* with 1xrDNA vs. 2xrDNA in G1 (top right map) vs.
470 late anaphase (bottom left map). Black arrowheads point at contact variations adjacent to the rDNA
471 loci. **c** Contact quantification between rDNA-flanking regions on chr *C*, as described in Figure 3b.
472 Relative percentages of contact reduction in anaphase compared to G1 are indicated for each strain
473 with one, two and no rDNA.

474 **Methods**

475 **Strains and culture conditions**

476 All strains used in this study are listed in Extended Data Table 1 and they are derived from BY4741
477 and BY4742 [55] by transformation events. Deletion of the entire open reading frame of *SIR2* gene
478 was performed using the CRISPR-Cas9 with a single gRNA and a ~1 kb-long repair donor
479 generated by fusion PCR on *SIR2*-flanking sequences. The thermosensitive mutation in *CDC15*
480 (*cdc15-2* ts) was introduce with CRISPR-Cas9. Oligos used in this study are listed in Extended
481 Data Table 4.

482 Strains were grown in rich medium (YPD: 1% bacto peptone (Difco), 1% bacto yeast extract
483 (Difco) and 2% glucose; YPG: 1% bacto peptone (Difco), 1% bacto yeast extract (Difco) and 3%
484 glycerol) or in synthetic complete medium (SC: 0.67% yeast nitrogen base without amino acids
485 (Difco), supplemented with a mix of amino-acids and 2% glucose). Cells were grown at either
486 30°C or 24°C, the latter corresponds to the permissive temperature of the conditional
487 thermosensitive mutant *cdc15-2* (see also methods in Lazar-Stefanita et al., 2022 in press).

488 **Serial dilution assay and growth curves**

489 Yeast cultures from independent isolates of *n*=16 WT rDNA (BY4741), *n*=3 rDNA *CEN* distal
490 (JL411), *n*=3 rDNA *CEN* proximal (JL665) and *n*=3 rDNA *CEN* proximal and distal (LS71) strains
491 were grown in YPD liquid medium at 30ºC to saturation. For serial dilution assay: yeast cultures
492 in stationary phase were diluted to A_{600} = 0.1 and serially diluted (1:10) in sterile water then spotted
493 on different media (YPD, YPG and SC) and incubated at different temperatures (30ºC and 37ºC)
494 for 2 days. For growth curves: yeast cultures in stationary phase were diluted in fresh YPD medium
495 to A_{600} = 0.05, 200 µl were transferred to 96 well plates and every minute the BioTek Eon
496 microplate spectrophotometer was programmed to shake the plate and measure the A_{600} for a total

497 of 24 h at 30ºC. A_{600} values were imported in GraphPad Prism version 9 for Mac OS (GraphPad
498 Software, San Diego, California USA, www.graphpad.com) and used to calculate mean and
499 standard deviation for each isolate of each strain. Doubling time was calculated using the slope of
500 the growth curves.

501 **rDNA Megablock engineering**

502 A CRISPR-Cas9 based method was used to promote during the cut-and-paste rDNA locus
503 relocation from the native location (flanked by chromosome 12 sequence) to an ectopic position
504 generated by fusing telomere 15R and telomere 4L. The method was performed as described by
505 Luo et al. *Nature* in 2018, except that two gRNAs cut the flanking regions of rDNA locus and the
506 third gRNA cuts at the new ectopic insertion site. In addition, three donor templates were generated
507 by fusion PCR, they include: (*i*) a donor template to rejoin the ends of the native locus upon rDNA
508 deletion, (*ii*) a donor template for bridging the left flanking region of the rDNA locus to its new
509 target location and (*iii*) a donor template for bridging the right flanking region of rDNA locus to
510 its new target location. rDNA translocation was verified by PCR with primer pairs designed
511 outside the newly formed chromosome junctions.

512 **Pulsed-field gel electrophoresis (PFGE) and Dual color Southern blot**

513 Chromosomes from stationary yeast cell cultures were prepared in agar molds using the Certified
514 Megabase Agarose (Bio-Rad CAT. 1613108) and pulsed-field gel electrophoresis (PFGE) was
515 carried out as previously described, with running conditions recommended for either *S. cerevisiae*
516 or *S. pombe* chromosomes. Specifically, megachromosomes were separated on a 0.8% agar gel in
517 1X TAE at 14ºC. Run time was ~72 h at 2V/cm with switch time of 20-30 min at an included angle
518 of 106º [16]. DNA size markers used were the *S. pombe* chromosomal DNA (Bio-Rad CAT. 170-
519 3633) and *H. wingei* chromosomal DNA (Bio-Rad CAT. 170-3667).

520 Method for chromosome digests: prior to BamHI (NEB CAT. R0136L) digestion, agar plugs were
521 equilibrated in 1X NEB3.1 restriction buffer for 24h at 4ºC. BamHI digest was carried out for 24
522 h at 37ºC in ~500 µl final volume consisting of: ~100 mg agar, 50 µl 10X restriction buffer and 10
523 µl BamHI enzyme (200 U). Agar molds treated with BamHI were then used for PFGE and
524 Southern blot.
525 The protocol for dual color Southern blot was optimized based on [56]. Following electrophoresis of
526 BamHI treated agar plugs, the gel was washed in: depurination solution (0.25M HCl) for 20 min,
527 denaturation solution (0.5M NaOH, 1.5M NaCl) for 60 min and neutralization solution (0.5M Tris,
528 1.5M NaCl pH 7.5) for 30 min. Chromosomes were transferred by capillarity to a nylon membrane
529 (Pall® 60208 Biodyne™ B Membrane, Pore Size 0.45 µm CAT. 60208) using 10X SSC buffer
530 (20X SSC: 1.5M NaCl, 0.3M Sodium citrate pH 7) for 72 h. After transfer the membrane was
531 washed with 2X SSC for 5 min and baked at 80ºC for 30 min. Prehybridization and hybridization
532 steps were performed at 50ºC in ULTRAhyb™ Ultrasensitive Hybridization Buffer (Invitrogen
533 Ambion CAT. AM8670). PCR products (~1.1 kb-long flanking unique sequences on either side of
534 each rDNA locus) were labelled using Klenow Fragment exo- (NEB CAT. M0212L) with either
535 Biotin-16-dUTP (Roche CAT. 11093070910) or Digoxigenin-11-dUTP alkali-stable (Roche CAT.
536 11093088910) at 37ºC for 1 hour. Labelled DNA probes were cleaned up using Zymo-Spin I
537 Columns (Zymo Research CAT. C1003-50), denaturated at 95ºC for 5 min and ~300 ng of each
538 were used for each hybridization experiment. The blot was washed twice with 2X SSPE buffer
539 (20X SSPE Buffer: 0.02M EDTA and 2.98M NaCl in 0.2M phosphate buffer pH 7.4; Sigma-
540 Aldrich CAT. S2015) for 5 min at room temperature; twice with 2X SSPE, 1% SDS for 30 min at
541 55ºC; twice with 0.1X SSPE for 15 min at 55ºC. Blot was incubated in Blocking buffer Odyssey

542 (LI-COR® CAT. 927-40000) in 1X Tris-Buffered Saline with 0.1% Tween 20 and 1% SDS for 3
543 h at room temperature.
544 The membrane was washed with 1X TBST for 5 min and incubated for 1 h at room temperature
545 with rabbit anti-DIG antibody (working concentration 1:2500 in Blocking buffer Odyssey;
546 ABfinity™ Rabbit Monoclonal, CAT. 700772). The primary antibody solution was washed out
547 three times with 1X TBST for 15 min at room temperature. The membrane was incubated in the
548 secondary antibody solution (working concentration 1:10000 in Blocking buffer Odyssey): Licor
549 IRDye® 800CW Streptavidin, 0.5 mg (CAT. 926-32230) and LIRDye® 680RD Goat anti-Rabbit
550 IgG (H + L), 0.5 mg (CAT. 926-68071) for 30 min at room temperature. Secondary antibody
551 solution was discarded and the membrane was washed three times with 1X TBST for 15 min at
552 room temperature before imaging acquisition using LI-COR Odyssey® Imager.

553 **Mating type switching**

554 Here we used the same reagents and protocol described by [42].

555 **Sporulation and tetrad dissection**

556 A detailed protocol for mating, sporulation and tetrad dissection of yeast with fused chromosomes
557 was described by Luo et al., 2018.

558 **RNA extractions**

559 Total RNA was extracted from 3 independent isolates of *n*=16 WT rDNA (BY4741), *n*=3 rDNA
560 *CEN* distal (JL411), *n*=3 rDNA *CEN* proximal (JL665) and *n*=3 rDNA *CEN* proximal and distal
561 (LS71) strains. Approximately $2x10^8$ cells were harvested from log phase cultures (1.5-2 $x10^7$
562 cells/ml) grown in YPD medium at 30ºC. Cell pellets were washed in RNase free water and
563 resuspended in RNA lysis buffer (50mM Tris-HCl pH 8, 100mM NaCl). Cells were lysed
564 mechanically using acid-washed glass beads (Sigma-Aldrich CAT. G8772-100G) at 4ºC. The

565 RNA was extracted by phenol:chloroform:isoamylalcohol (ThermoFisherScientific CAT. 15593)
566 and ethanol precipitated. Extractions were treated with DNaseI (Agilent CAT. 600031) for 1 hour
567 at 37ºC and RNA quality was verified by agarose gel in 1X TAE.

568 **RT-qPCR**

569 The above total RNA extractions were serial diluted (1:10/100/1000) and used for RTqPCR
570 reactions with gene specific oligos (18S, 25S and TAF10). The reverse transcriptase (RT) reaction
571 was performed according to the manufacturer protocol SuperScript™ IV Reverse Transcriptase
572 (Invitrogen CAT. 18090050). Successively, quantitative PCR was performed using the
573 LightCycler® 480 SYBR Green I Master (Roche CAT. 04887352001) and the standard
574 amplification protocol with 45 cycles in a multi-well PCR plate 384. Ct values for each replicate
575 were imported in GraphPad Prism version 9 for Mac OS (GraphPad Software, San Diego,
576 California USA, www.graphpad.com) and used to calculate mean and standard deviation for each
577 gene in each strain. The three plots generated, that correspond to each gene, show Ct variation in
578 function of the RNA dilution factor and strain.

579 **RNA library preparation, sequencing and analysis**

580 Stranded total RNA-seq libraries were prepared with the QIAseq stranded RNA library kit
581 (Qiagen, CAT. 180743) following the manufacture's recommendations using dual indexing
582 primers. Additionally, the input total RNA was first processed with the QIAseq FastSelect rRNA
583 Yeast kit to remove cytoplasmic and mitochondrial rRNA (Qiagen, CAT. 334215). Library quality
584 was assessed using the ZAG 110 dsDNA kit on (Agilent, CAT. ZAG-110-5000) and run on the
585 ZAG DNA analyzer system (Agilent). Libraries were then sequenced on an Illumina NextSeq 500
586 using the 75-cycle high output in paired end mode (Illumina, CAT. 20024906).

587 Differential gene analysis (Extended Data Table 2). RNA sequencing analysis was performed as
588 previously described [57] using kallisto/sleuth suite with minor modifications. Briefly, reads were
589 processed by Illumina barcode and quality trimming with Trimmomatic [58] and quality assessed
590 with FastQC. Next, reads were aligned using the pseudo-alignment program kallisto [59] to the
591 reference S288C genome [60], with annotations supplied with a gtf file containing all annotated
592 RNAs in stranded paired end mode (options, --genomebam --gtf --fr-stranded). The output of
593 kallisto was then used for data analysis in sleuth [61]. Volcano plots were generated using the Walds
594 test false discovery rate adjusted *P* value ($p<0.01$) and log2 fold change ($-2>Log2FC>2$).

595 **Cell cycle synchronization**

596 For both imaging and Hi-C experiments yeast cells, carrying either a single rDNA locus (LS88,
597 LS95) or two rDNA loci in *cis* (LS90, LS103), were synchronized in either G1 with alpha-factor
598 (Zymo Research, CAT. Y1001), or in late anaphase, using the thermosensitive mutant *cdc15-2*.
599 Method for G1 synchronization (LS88 and LS90): cells were grown to saturation in 5 ml SC
600 medium at 30ºC, the next day cells were subcultured in 150 ml fresh SC medium (A_{600}=0.5) for 2
601 h 30 min at 30ºC then alpha-factor was added (final concentration: 25 μM) and cultures were
602 incubated for additional 2 h 30 min at 24ºC before imaging and formaldehyde crosslink.
603 Method for late anaphase synchronization (LS95 and LS103): cells were grown to saturation in 5
604 ml SC medium at 24ºC, the next day they were subcultured in 150 ml fresh SC medium (A_{600}=0.5)
605 and grown for 5 h at 24ºC then the temperature was switched to 37ºC (non-permissive condition)
606 and incubated for additional 3 h before imaging and formaldehyde crosslink.
607 The quality of G1 and anaphase synchronizations was visually monitored by microscopy hourly.
608 For microscopy small aliquots (~1-2 ml synchronized cultures) were spooned down at 3000g for

609 3 min and fixed in ethanol 70%; whereas, the remaining cultures were fixed with formaldehyde
610 for Hi-C library preparation (see below).

611 **Protein tagging and imaging of the nucleolus**

612 The cell cycle reorganization of the nucleolus within the nucleus was monitored using
613 fluorescently tagged proteins at their endogenous C-terminus. Nuclear envelope was labelled with
614 either mCherry (*NIC96::mCherry*) or mScarlet (*NUP49::mScarlet*), while the nucleolus with GFP
615 (*NOP10::EGFP*) as described by [42](see also strain genotype in Extended Data Table 1). Imaging
616 was performed on the EVOS M7000 microscope using the Olympus X-APO 100 Oil, 1.45NA/WD
617 0.13mm (Oil) objective. Images were acquired as Z-stacks and visualized as max intensity
618 projections using ImageJ [62].

619 **Hi-C library preparation and data analysis**

620 Hi-C libraries (Extended Data Table 3) were prepared from yeast cells harvested from either log
621 phase or cell cycle synchronized cultures (see above protocols for cell synchronizations). Methods
622 for yeast Hi-C library preparation and data analysis were performed as previously described by
623 Lazar-Stefanita et al., 2017; 2022. Briefly, Hi-C reads were aligned using Bowtie 2 [63] and
624 processed using command lines based on HiCLib tool developed in the Mirny lab (Imakaev et al.,
625 2012). Normalized contact maps (Sequential Component Normalization, [64] were 5 kb-binned and
626 were plotted using MatLab R2018 (The MathWorks, Inc., Natick, Massachusetts, United States).
627 The Hi-C assay resulted crucial to validate the transplantation of the rDNA locus. We found that
628 among the potential candidates - that were PCR positive for the rDNA transplantation - only one
629 isolate had the entire locus relocated that resulted in the actual re-positioning of the rDNA
630 boundary from the native location (centromere-distal: 2.75 Mb from the active centromeric
631 sequence, *CEN15,* and 0.6 Mb from the nearest telomeric sequence, *TEL12R*) to the new ectopic

632 position at the fusion junction between the left arm of former chromosome *15* and the right arm of
633 former chromosome *4* (centromere-proximal: 0.75 Mb from *CEN15* and 2.52 Mb from *TEL12R*).
634 Of note, in the isolates that were false positives by PCR for the rDNA megablock transplantation,
635 the chromosome boundary formed by this locus remained at the original location (centromere-
636 distal) as expected.
637 The Hi-C maps were used to evaluate the strength of each rDNA boundary in function of their
638 distance from the centromere and locus number (single vs. double) across megachromosome *C*.
639 For this analysis we firstly reasoned that the chromosome boundaries observed at the location of
640 the rDNA loci on the 2D maps are 'visual artifacts' due to the combination of different structural
641 characteristics at this locus. Indeed, the highly repetitive nature and the formation of a subnuclear
642 compartment (nucleolus) appear to lower the contact frequency between the rDNA-flanking
643 regions. Along the same lines we also expected that differences in structure and/or size between
644 rDNA loci would have an effect on the strength of the correspondent chromosome boundaries. In
645 other words, bigger the rDNA locus ('bulkier' the nucleolus) lower the contact frequency between
646 its flanking sequences, therefore stronger the boundary. To compare between the *CEN* proximal
647 and *CEN* distal rDNA boundaries, located in single or double copy on megachromosome *C*, we
648 used normalized maps (5 kb-binned) to quantify contacts between 500 kb-long regions (flanking
649 either the right or the left end of each locus) and the 1.9 Mb region upstream/downstream or
650 enclosed by two loci (see highlighted regions in blue on chr *C* maps in Figure 3a). Spread point
651 plots, where each point corresponds to total contacts made by each 5 kb bin, were generated for
652 each rDNA boundary using Matlab. *P* values were calculated using the Kolmogorov–Smirnov test
653 (K–S test) function in MATLAB 2018a (The MathWorks, Inc., Natick, Massachusetts, United
654 States).

Log2 ratios of Hi-C contact maps were used for their pairwise comparison and the contact probability decay in function of the genomic distance, $p(s)$, was computed to assess the status of the chromatin fiber. Both these analyses were performed as previously described by Lazar-Stefanita et al., 2017; 2022 in press.

Acknowledgments

We acknowledge all members of Boeke lab for their assistance. We thank Aleksandra Wudzinska and Gregory Goldberg for their comments on the manuscript. This work was supported by National Science Foundation grants MCB-1616111 and MCB-1921641 and NIH grant RM1HG009491 to JDB.

Author Contributions

LLS and JDB designed the research project. LLS performed the experiments with help from: JL that relocated the rDNA array, WZ that built *n*=16 with rDNA on heterologous chromosomes and MH that performed and analyzed RNAseq. LLS wrote the manuscript and all authors contributed to editing.

Additional Information

Genome-wide and RNA sequencing files were deposited at the NCBI database as FASTQ files. See BioProject accession number PRJNA847233 for the SRA data. The reviewer link: https://dataview.ncbi.nlm.nih.gov/object/PRJNA847233?reviewer=6h4lqpu2o2epg0f4ta40dlmqo4

Competing interests

Jef Boeke is a Founder and Director of CDI Labs, Inc., a Founder of Neochromosome, Inc, a Founder of and Consultant to ReOpen Diagnostics, and serves or served on the Scientific Advisory Board of the following: Modern Meadow, Inc., Rome Therapeutics, Inc., Sample6, Inc., Sangamo, Inc., Tessera Therapeutics, inc., and the Wyss Institute. The remaining authors declare no competing interests.

Extended Data Tables and Figures

Title: Stable twin rDNA loci form a single nucleolus in brewer's yeast

Authors

Luciana Lazar-Stefanita[1], Jingchuan Luo[1†], Max A. B. Haase[1,2], Weimin Zhang[1], Jef D. Boeke[1,3]*

*, Corresponding author: jef.boeke@nyulangone.org

Affiliations

[1] Institute for Systems Genetics and Department of Biochemistry and Molecular Pharmacology, NYU Langone Health, New York, NY 10016, USA

[2] Vilcek Institute of Graduate Biomedical Sciences at NYU School of Medicine

[3] Department of Biomedical Engineering, NYU Tandon School of Engineering, Brooklyn NY 11201 USA

† Present address: Whitehead Institute for Biomedical Research, Cambridge, MA, 02142, USA

16 **Extended Data Tables:**

17 Extended Data Table 1 List of strains used in this study.

18 Extended Data Table 2 RNA seq. list of differentially expressed genes.

19 Extended Data Table 3 Hi-C libraries.

20 Extended Data Table 4 Primers list used in this study.

21

22 **Extended Data Figures and Figure Legends:**

23 Extended Data Figure 1 rDNA locus transplantation and duplication at ectopic chromosomal

24 locations.

25 Extended Data Figure 2 Effects of rDNA duplication on genome stability and cell fitness.

26 Extended Data Figure 3 Stability of the rDNA locus in function of chromosome position and

27 silencing.

28 Extended Data Figure 4 Cell cycle reorganization of the chromosome with twin rDNA loci in *cis*.

29 Extended Data Figure 5 Duplicated rDNA loci may lead chromosome mispairing in meiosis.

30

31 **Extended Data Tables**

Strain name	Parent	Genotype	Nr. Chr.	rDNA location	Ref.
BY4741	S288C	*MAT**a** his3Δ1 leu2Δ0 met15Δ0 ura3Δ0*	16	Chr *12*	(Brachmann et al., 1998)
WZ456	BY4742	*MAT**a** his3Δ1 leu2Δ0 lys2Δ0 ura3Δ0 rdn::C-S.ITS-LEU2 NOP10::EGFP-KanMX, NIC96::mCherry-HIS3*	16	Chr *12*	(Zhang et al., 2017)
WZ457	BY4742	*MAT**a** his3Δ1 leu2Δ0 lys2Δ0 ura3Δ0 rdn::NatMX4 NOP10::EGFP-KanMX, NIC96::mCherry-HIS3 YCR018C / C-S.ITS-LEU2 / YCR019W*	16	Chr *3*	(Zhang et al., 2017)
WZ499	Spore of yWZ456 X yWZ457	*MAT**a** his3Δ1 leu2Δ0 lys2Δ0 ura3Δ0 rdn::C-S.ITS-LEU2 NOP10::EGFP-KanMX, NIC96::mCherry-HIS3, YCR018C / C-S.ITS-LEU2 / YCR019W*	16	Chr *12* + Chr *3*	(Zhang et al., 2017)
JL411	BY4741	*MAT**a** his3Δ1 leu2Δ0 met15Δ0 ura3Δ0*	3	Chr *C* distal	(Luo et al., 2018a)
JL665	JL411	*MAT**a** his3Δ1 leu2Δ0 met15Δ0 ura3Δ0*	3	Chr *C* proximal	This work
LS88	JL665	*MAT**a** his3Δ1 leu2Δ0 met15Δ0 ura3Δ0 NOP10::EGFP-KanMX NUP49::mScarlet-S.p.HIS5*	3	Chr *C* proximal	This work
LS95	LS88	*MAT**a** his3Δ1 leu2Δ0 met15Δ0 ura3Δ0 cdc15-2(Ts) NOP10::EGFP-KanMX NUP49::mScarlet-S.p.HIS5*	3	Chr *C* proximal	This work
LS70	JL665 X JL411	*MAT**a/alpha** his3Δ1/ his3Δ1 leu2Δ0/ leu2Δ0 met15Δ0/met15Δ0 ura3Δ0/ura3Δ0*	3	Chr *C* proximal & Chr *C* distal	This work
LS71-C1&C2	Spore of LS70	*MAT**alpha** his3Δ1 leu2Δ0 met15Δ 0ura3Δ0*	3	Chr *C* proximal + distal	This work
LS71-C3	Spore of LS70	*MAT**a** his3Δ1 leu2Δ0 met15Δ0 ura3Δ0*	3	Chr *C* proximal + distal	This work
LS90	LS71-C3	*MAT**a** his3Δ1 leu2Δ0 met15Δ0 ura3Δ0 NOP10::EGFP-KanMX NUP49::mScarlet-S.p.HIS5*	3	Chr *C* proximal + distal	This work
LS91	Haploids of JL411	*MAT**a/alpha** his3Δ1/ his3Δ1 leu2Δ0/ leu2Δ0 met15Δ0/met15Δ0 ura3Δ0/ura3Δ0*	3	Chr *C* distal & Chr *C* distal	This work

LS92	Haploids of JL665	*MAT**a/alpha** his3Δ1/ his3Δ1 leu2Δ0/ leu2Δ0 met15Δ0/met15Δ0 ura3Δ0/ura3Δ0*	3	Chr *C* proximal & Chr *C* proximal	This work
LS93	LS71-C1 X LS71-C3	*MAT**a/alpha** his3Δ1/ his3Δ1 leu2Δ0/ leu2Δ0 met15Δ0/met15Δ0 ura3Δ0/ura3Δ0*	3	Chr *C* proximal + distal & Chr *C* proximal + distal	This work
LS103	LS90	*MAT**a** his3Δ1 leu2Δ0 met15Δ0 ura3Δ0 cdc15-2(Ts) NOP10::EGFP-KanMX NUP49::mScarlet-S.p.HIS5*	3	Chr *C* proximal & distal	This work
LS130 (LS131)	JL411	*MAT**a** his3Δ1 leu2Δ0 met15Δ0 ura3Δ0 sir2Δ*	3	Chr *C* distal	This work
LS141 (LS142)	Diploid (*SIR2/ sir2Δ*)	*MAT**a** or **alpha** his3Δ1 leu2Δ0 met15Δ0 ura3Δ0 sir2Δ*	3	Chr *C* proximal & distal	This work
LS143 (LS144)	Diploid (*sir2Δ/ sir2Δ*)	*MAT**a** or **alpha** his3Δ1 leu2Δ0 met15Δ0 ura3Δ0 sir2Δ*	3	Chr *C* proximal & distal	This work

Extended Data Table 1 List of strains used in this study.

Extended Data Table 2 RNA seq. list of differentially expressed genes.

Data presented as excel spreadsheet file.

Strain name	**Karyotype (n, #rDNA-position)**	**Synchronization method**	**Total paired-end reads**	**Aligned paired-end reads**	**Total contacts in 5 kb-binned maps**
JL411	3, 1-distal	none	24770805	19642950	5273769
JL665	3, 1-proximal	none	24447393	19581599	3662044
LS70	3, 1-distal + 1-prox	none	34383730	27174746	4918384
LS71-C1	3, 1-distal + 1-prox	none	29910065	20997502	3292606
LS71-C2	3, 1-distal + 1-prox	none	26807590	18886934	3585706

LS71-C3	3, 1-distal + 1-prox	none	32026043	23014301	4020070
LS88	3, 1-proximal	G1	12605198	8902009	5362318
LS90	3, 1-distal + 1-prox	G1	8820734	5893335	4041830
LS95	3, 1-proximal	Anaphase *cdc15-2*	12933900	9479614	6106239
LS103-C1	3, 1-distal + 1-prox	Anaphase *cdc15-2*	15026254	10109053	3904083
LS103-C2	3, 1-distal + 1-prox	Anaphase *cdc15-2*	28339485	20719596	4170357

Extended Data Table 3 Hi-C libraries. For each library it reports: number of chromosomes per strain, number of rDNA per chromosome, synchronization method and total Hi-C contacts.

Extended Data Table 4 Primers list used in this study.

Data presented as excel spreadsheet file.

42 **Extended Data Figure 1 rDNA locus transplantation and duplication at ectopic chromosomal**

43 **locations.**

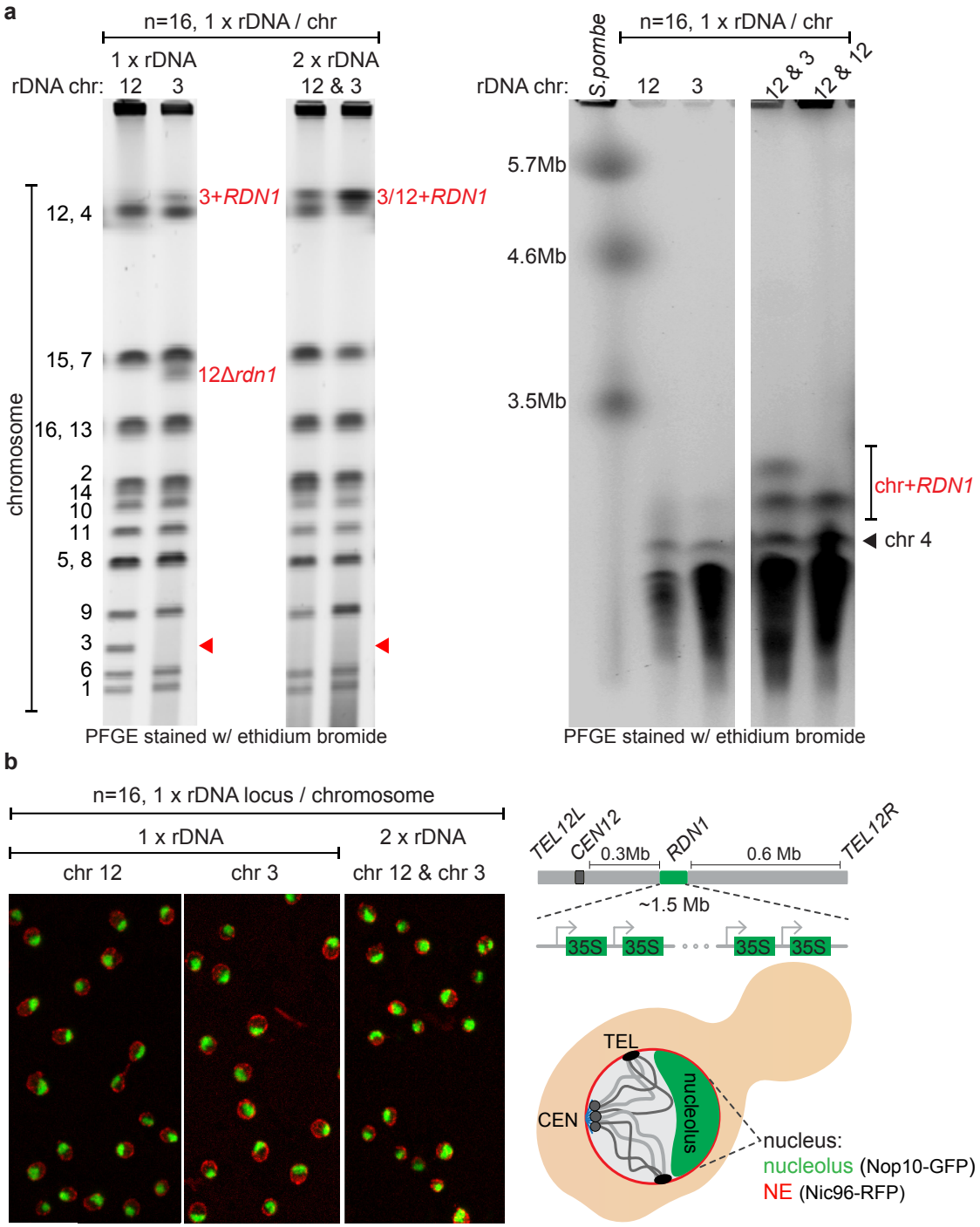

44

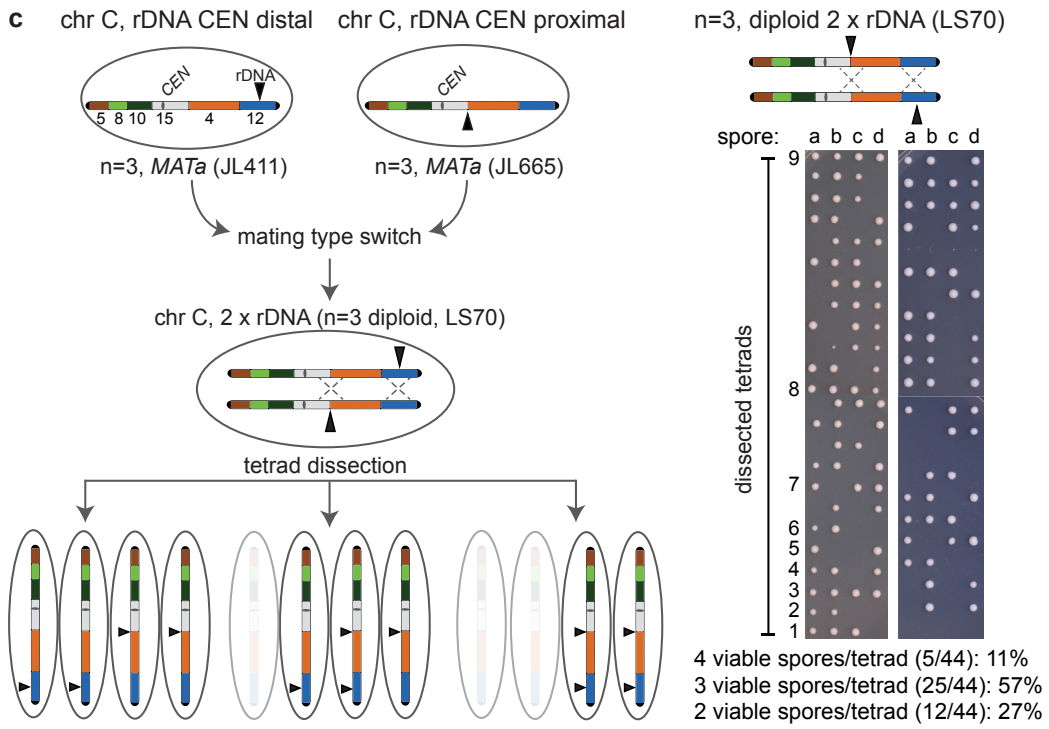
c
chr C, rDNA CEN distal
chr C, rDNA CEN proximal
n=3, diploid 2 x rDNA (LS70)
CEN
rDNA
5 8 10 15 4 12
n=3, MATa (JL411)
n=3, MATa (JL665)
mating type switch
chr C, 2 x rDNA (n=3 diploid, LS70)
tetrad dissection
spore: a b c d a b c d
dissected tetrads
9
8
7
6
5
4
3
2
1
4 viable spores/tetrad (5/44): 11%
3 viable spores/tetrad (25/44): 57%
2 viable spores/tetrad (12/44): 27%

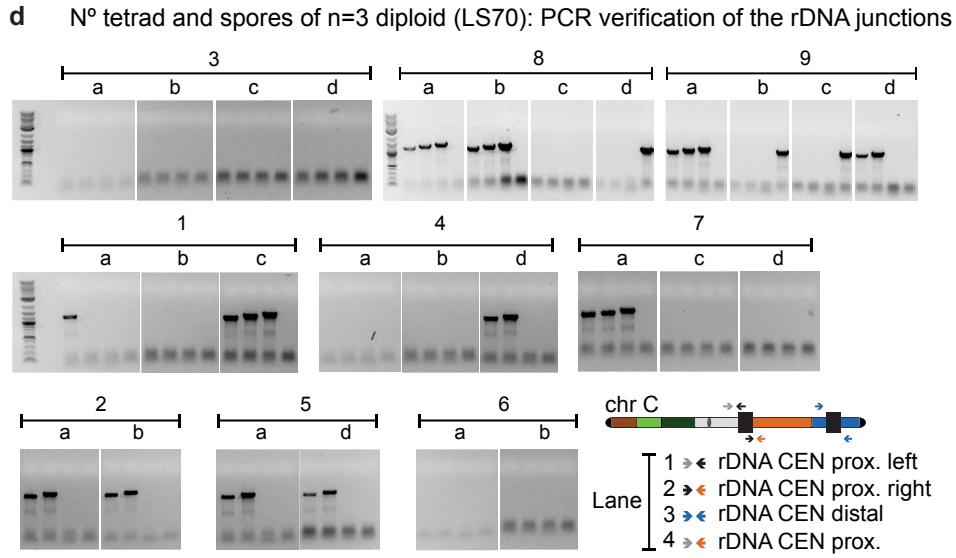
d
Nº tetrad and spores of n=3 diploid (LS70): PCR verification of the rDNA junctions
3
a b c d
8
a b c d
9
a b c d
1
a b c
4
a b d
7
a c d
2
a b
5
a d
6
a b
chr C
Lane
1 rDNA CEN prox. left
2 rDNA CEN prox. right
3 rDNA CEN distal
4 rDNA CEN prox.

46 **Extended Data Figure 1 rDNA locus transplantation and duplication at ectopic chromosomal**
47 **locations.**
48 **a** Chromosome separation by PFGE of wild-type yeasts with 16 chromosomes (*n*=16) with single
49 or two rDNA loci on different chromosomes (red indicates chromosomes that have lost or gain the
50 rDNA locus). Two distinct programs are used for chromosome separation: *S. cerevisiae* on the left
51 and *S. pombe* on the right. **b** Representative microscopy images of yeast nuclei with single or two
52 rDNA loci as described in Figure 1a,b. **c** Diagram showing the strategy used to duplicate the rDNA
53 locus within the same arm of megachromosome *C* in *n*=3 (chr *C* is colorcoded according to the
54 chromosome fusion design). Right panels show spores of individual tetrads (asci) of *n*=3 diploid
55 with two rDNA loci in asymmetric *trans* locations. **d** Verification of rDNA duplication by junction
56 PCR, sampling 4 different sequences in 27 spores originated from 9 different tetrads. Positive
57 spores for rDNA duplication show PCR products in lane 1 and 2 only.
58

59 **Extended Data Figure 2 Effects of rDNA duplication on genome stability and cell fitness.**

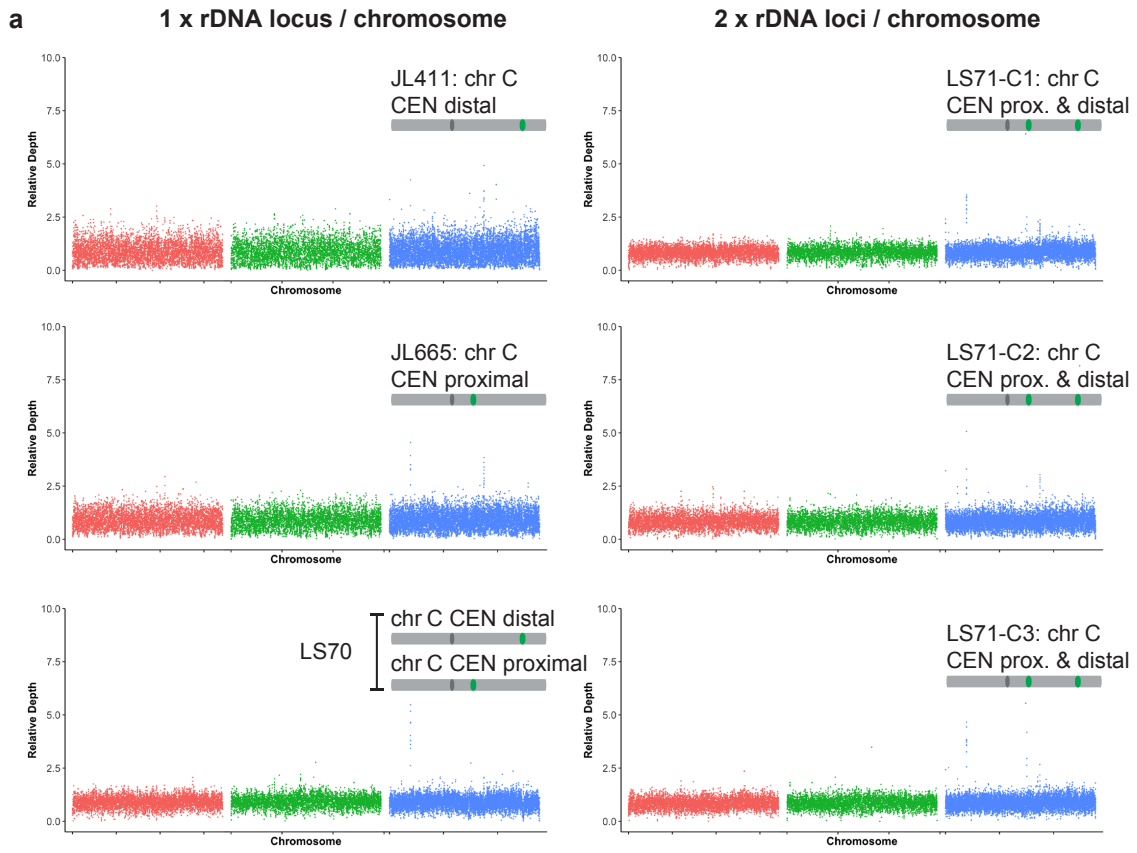

60

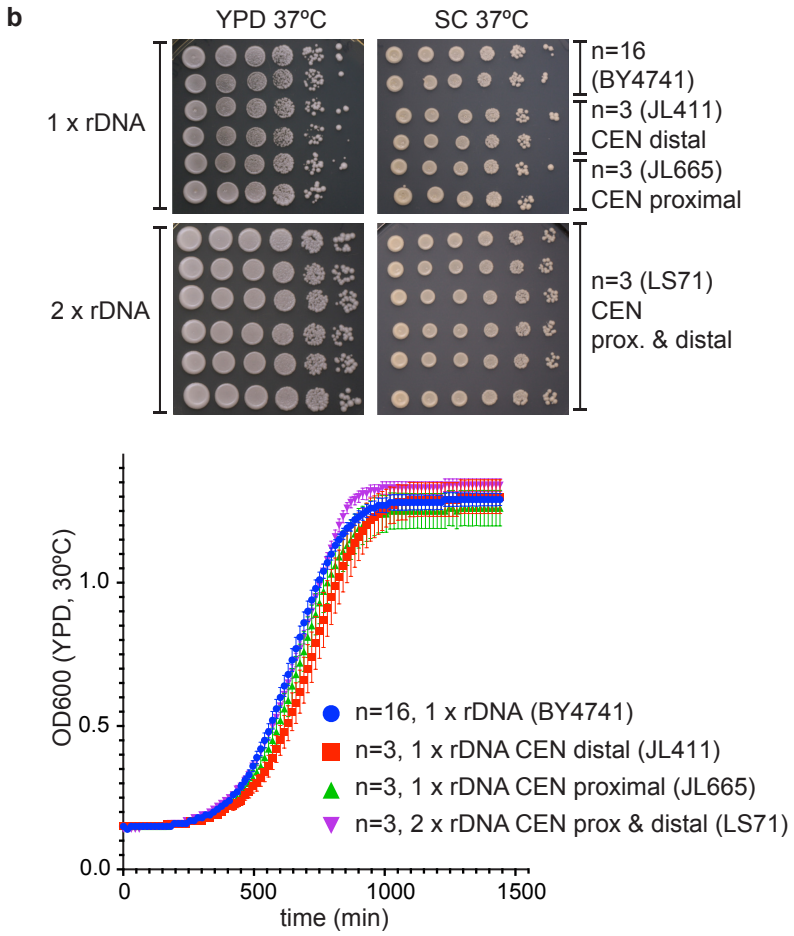
b
YPD 37ºC
SC 37ºC
1 x rDNA
2 x rDNA
n=16
(BY4741)
n=3 (JL411)
CEN distal
n=3 (JL665)
CEN proximal
n=3 (LS71)
CEN
prox. & distal
OD600 (YPD, 30ºC)
0.0
0.5
1.0
0
500
1000
1500
time (min)
n=16, 1 x rDNA (BY4741)
n=3, 1 x rDNA CEN distal (JL411)
n=3, 1 x rDNA CEN proximal (JL665)
n=3, 2 x rDNA CEN prox & distal (LS71)

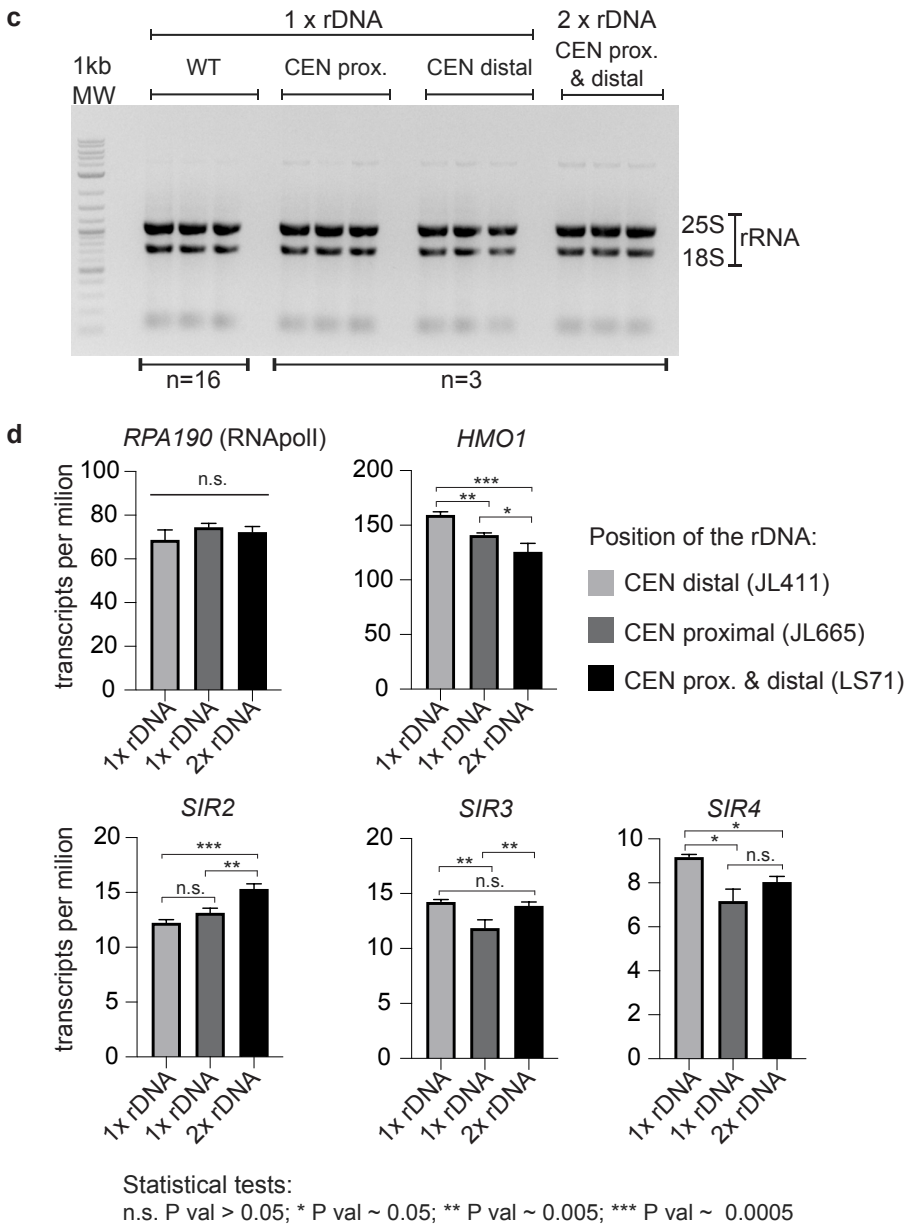
c
1 x rDNA
2 x rDNA
1kb MW
WT
CEN prox.
CEN distal
CEN prox. & distal
25S
18S
rRNA
n=16
n=3
d
RPA190 (RNApolI)
HMO1
SIR2
SIR3
SIR4
transcripts per milion
n.s.
1x rDNA
2x rDNA
Position of the rDNA:
CEN distal (JL411)
CEN proximal (JL665)
CEN prox. & distal (LS71)
Statistical tests:
n.s. P val > 0.05; * P val ~ 0.05; ** P val ~ 0.005; *** P val ~ 0.0005

63 **Extended Data Figure 2 Effects of rDNA duplication on genome stability and cell fitness.**

64 **a** Relative genome sequencing depth plots (ggplot2 function in R) of *n*=3 strains with a single
65 rDNA locus on chr *C* (haploids: JL411 and JL665 with either *CEN* distal or *CEN* proximal locus,
66 respectively; diploid: LS70 with *CEN* distal and proximal) or two loci on chr *C* (independent
67 haploids: LS71 C1 to C3). Sequencing depth for each megachromosome is colorcoded differently;
68 chr *C* is displayed on the top right of each plot. **b** Fitness assays of *n*=16 and *n*=3 isolates. Top
69 panels: serial dilution assays on different growing conditions at 37ºC see also Figure 2b. Bottom
70 panel: growth curves reporting optical densities (A600) in YPD at 30ºC. **c** Agarose gel reporting
71 the quality of the total RNA extracted from *n*=16 and *n*=3 isolates with different rDNA number
72 and position relative to Figure 2c. **d** Bar plots showing transcriptional changes of a specific subset
73 of genes (mainly involved in the metabolism of rRNA) in *n*=3 with a different number and position
74 of the rDNA locus see also Figure 2d.

75

76 **Extended Data Figure 3 Stability of the rDNA locus in function of chromosome position and**

77 **silencing.**

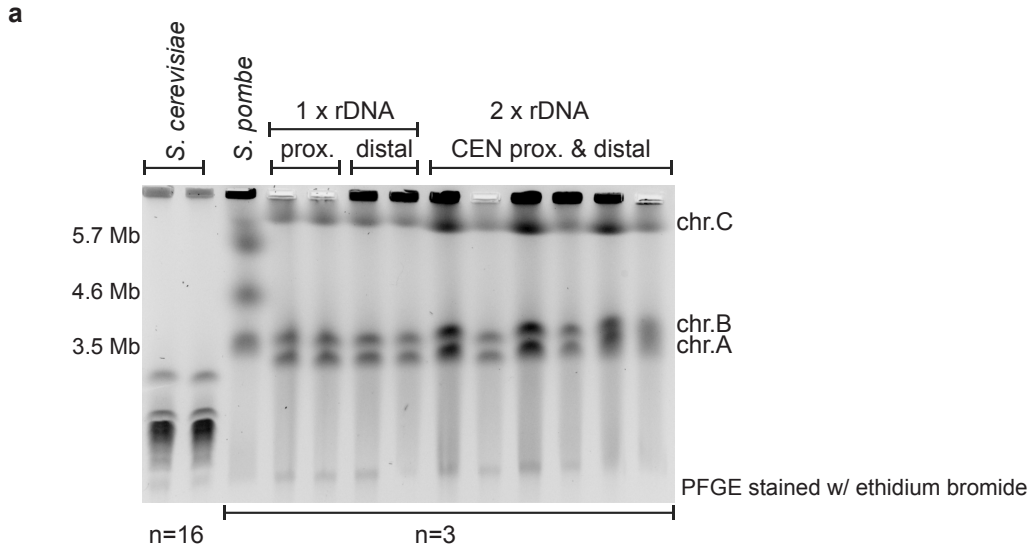

78

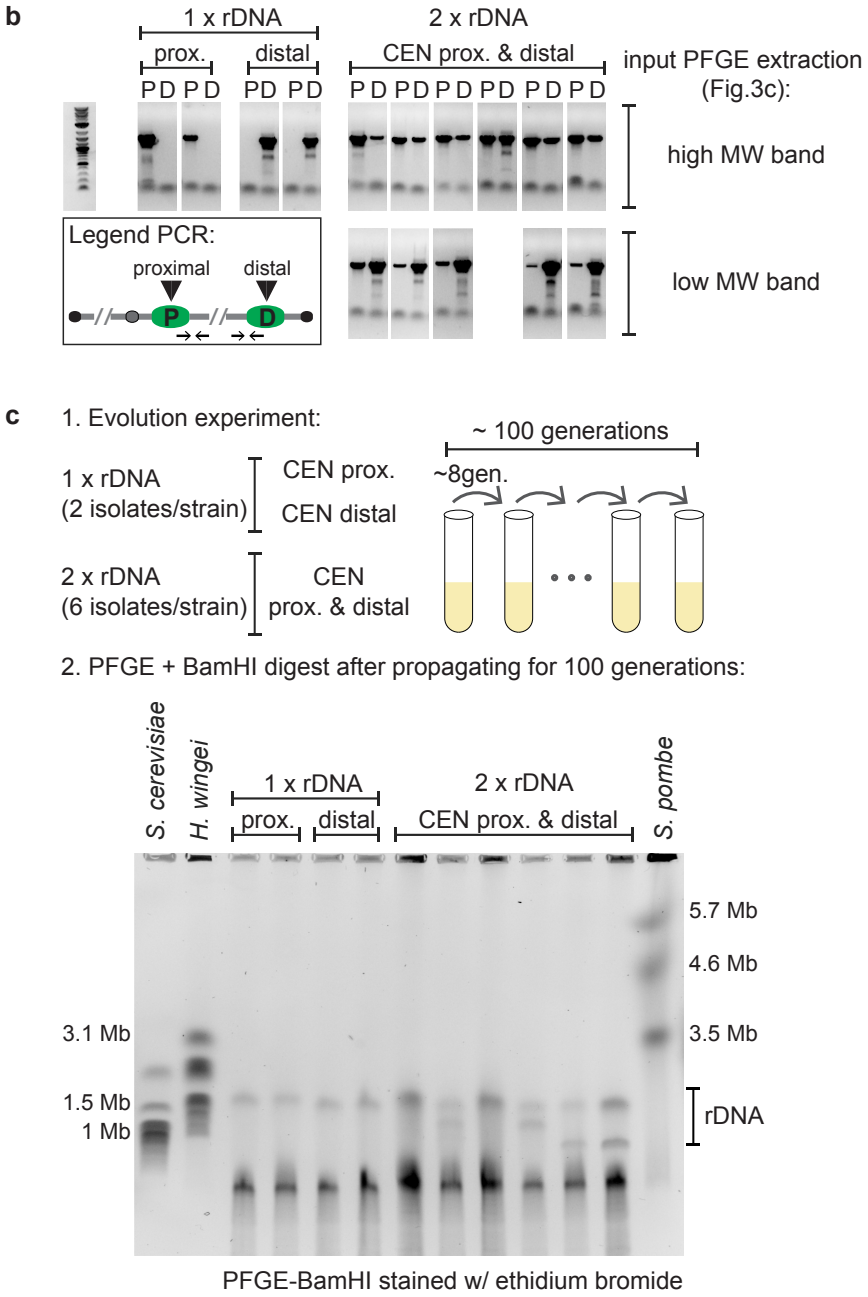
b
1 x rDNA
2 x rDNA
prox.
distal
CEN prox. & distal
P D P D
P D P D
P D P D P D P D P D P D
input PFGE extraction
(Fig.3c):
high MW band
low MW band
Legend PCR:
proximal
distal
P
D
c
1. Evolution experiment:
~ 100 generations
~8gen.
1 x rDNA
(2 isolates/strain)
CEN prox.
CEN distal
2 x rDNA
(6 isolates/strain)
CEN
prox. & distal
2. PFGE + BamHI digest after propagating for 100 generations:
S. cerevisiae
H. wingei
1 x rDNA
2 x rDNA
prox.
distal
CEN prox. & distal
S. pombe
5.7 Mb
4.6 Mb
3.1 Mb
3.5 Mb
1.5 Mb
1 Mb
rDNA
PFGE-BamHI stained w/ ethidium bromide

79

80

d

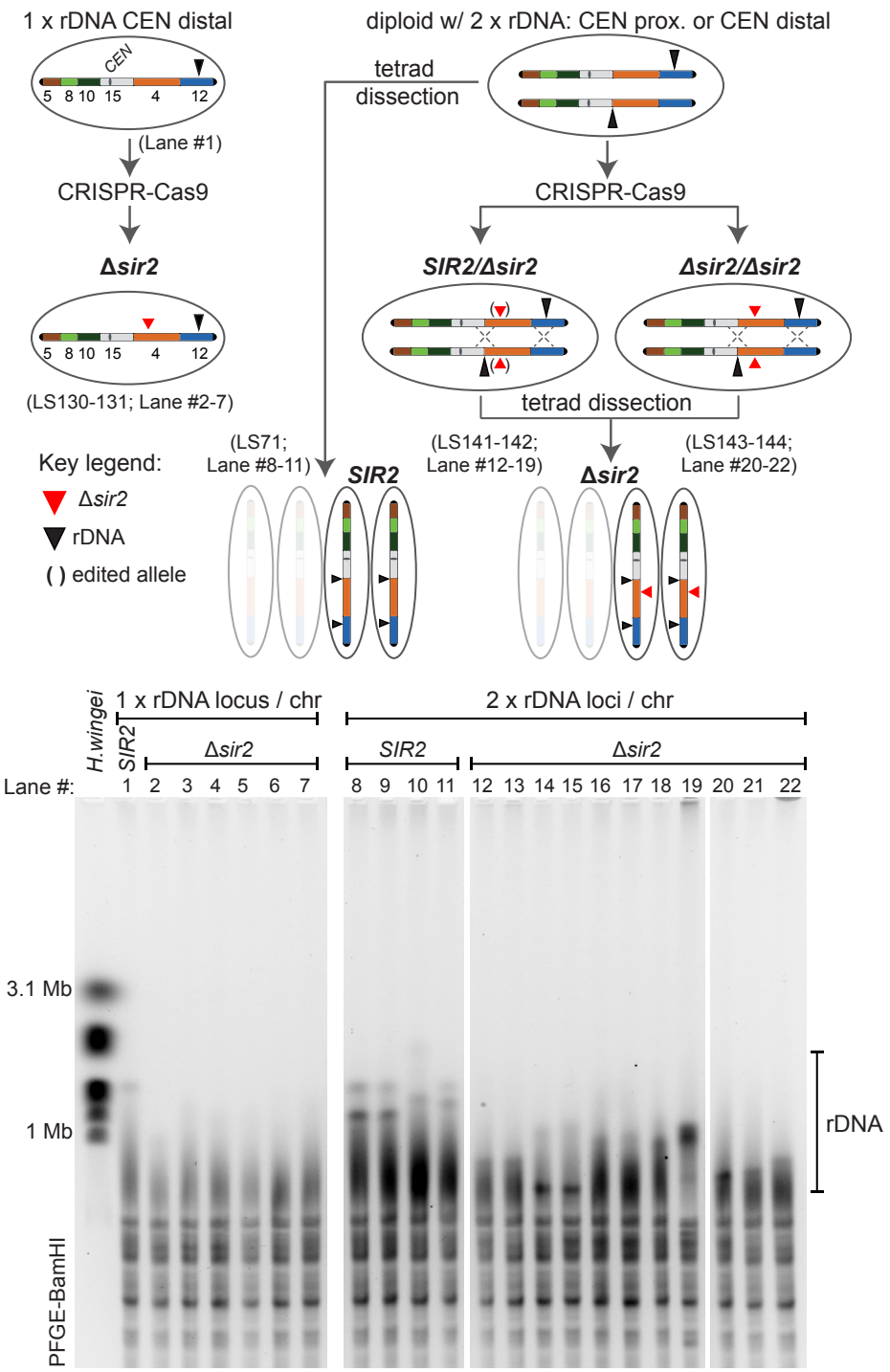
1 x rDNA CEN distal
diploid w/ 2 x rDNA: CEN prox. or CEN distal
CEN
5 8 10 15 4 12
(Lane #1)
tetrad dissection
CRISPR-Cas9
Δsir2
SIR2/Δsir2
Δsir2/Δsir2
(LS130-131; Lane #2-7)
tetrad dissection
(LS71; Lane #8-11)
(LS141-142; Lane #12-19)
(LS143-144; Lane #20-22)
Key legend:
Δsir2
rDNA
( ) edited allele
SIR2
Δsir2
H.wingei
1 x rDNA locus / chr
2 x rDNA loci / chr
SIR2
Δsir2
SIR2
Δsir2
Lane #:
1 2 3 4 5 6 7 8 9 10 11 12 13 14 15 16 17 18 19 20 21 22
3.1 Mb
1 Mb
PFGE-BamHI
rDNA

82 **Extended Data Figure 3 Stability of the rDNA locus in function of chromosome position and**
83 **silencing.**
84 **a** Chromosome separation by PFGE of different isolates of *n*=16 and *n*=3 strains, with either one
85 or two rDNA loci. PFGE run specifications: *S. pombe* program for mega-size chromosome
86 separation. **b** PCR-validations of rDNA proximal (P) and distal (D) junctions. DNA template
87 extracted from PFGE, rDNA bands that migrated at high or low molecular weights in Figure 3c. **c**
88 Schematics of the evolution experiment in *n*=3 strains with a different number and position of the
89 rDNA locus. Cell populations from different isolates were evolved long-term (~100 generations)
90 in batch cultures and used to assess the size of the rDNA arrays using PFGE and BamHI digest.
91 PFGE program as described in panel (a). **d** Diagram of the approach used to assess rDNA array
92 stability in function of Sir2. CRISPR-Cas9 was used to delete *SIR2* gene in *n*=3 haploid with one
93 rDNA locus, and in the diploid with two rDNA loci in *trans* and asymmetric. Haploid spores with
94 two *cis* rDNA loci obtained from sporulation of different diploids (*SIR2/SIR2, SIR2/sir2, sir2/sir2*)
95 were used to assess stability of the rDNA arrays by PFGE and BamHI digest. PFGE program as
96 described in panel (a).
97

98 **Extended Data Figure 4 Cell cycle reorganization of the chromosome with twin rDNA loci**

99 **in *cis*.**

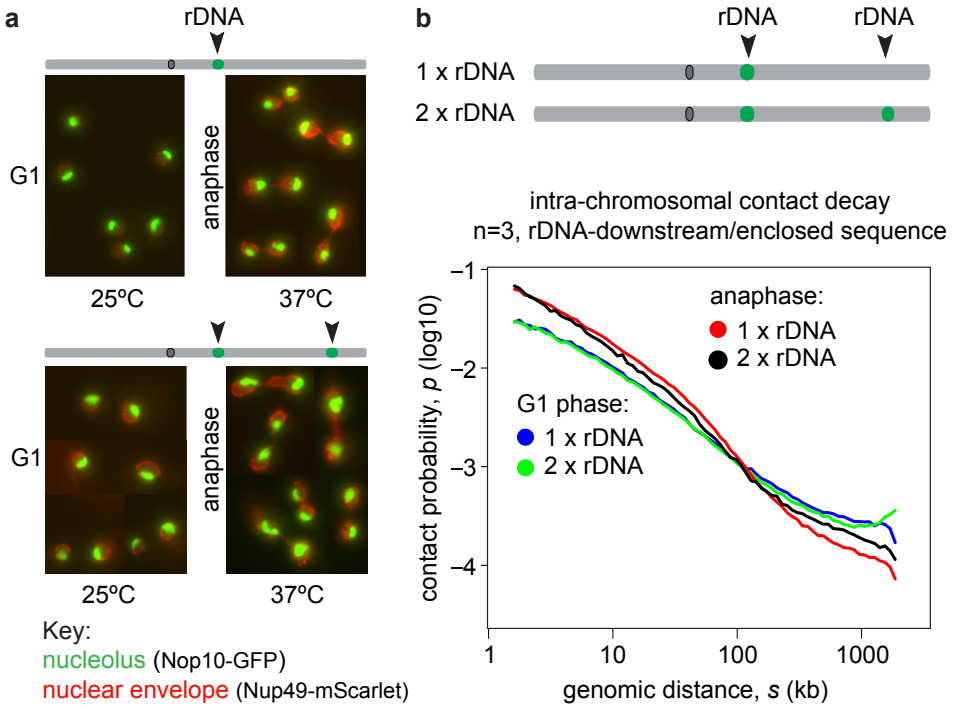

100

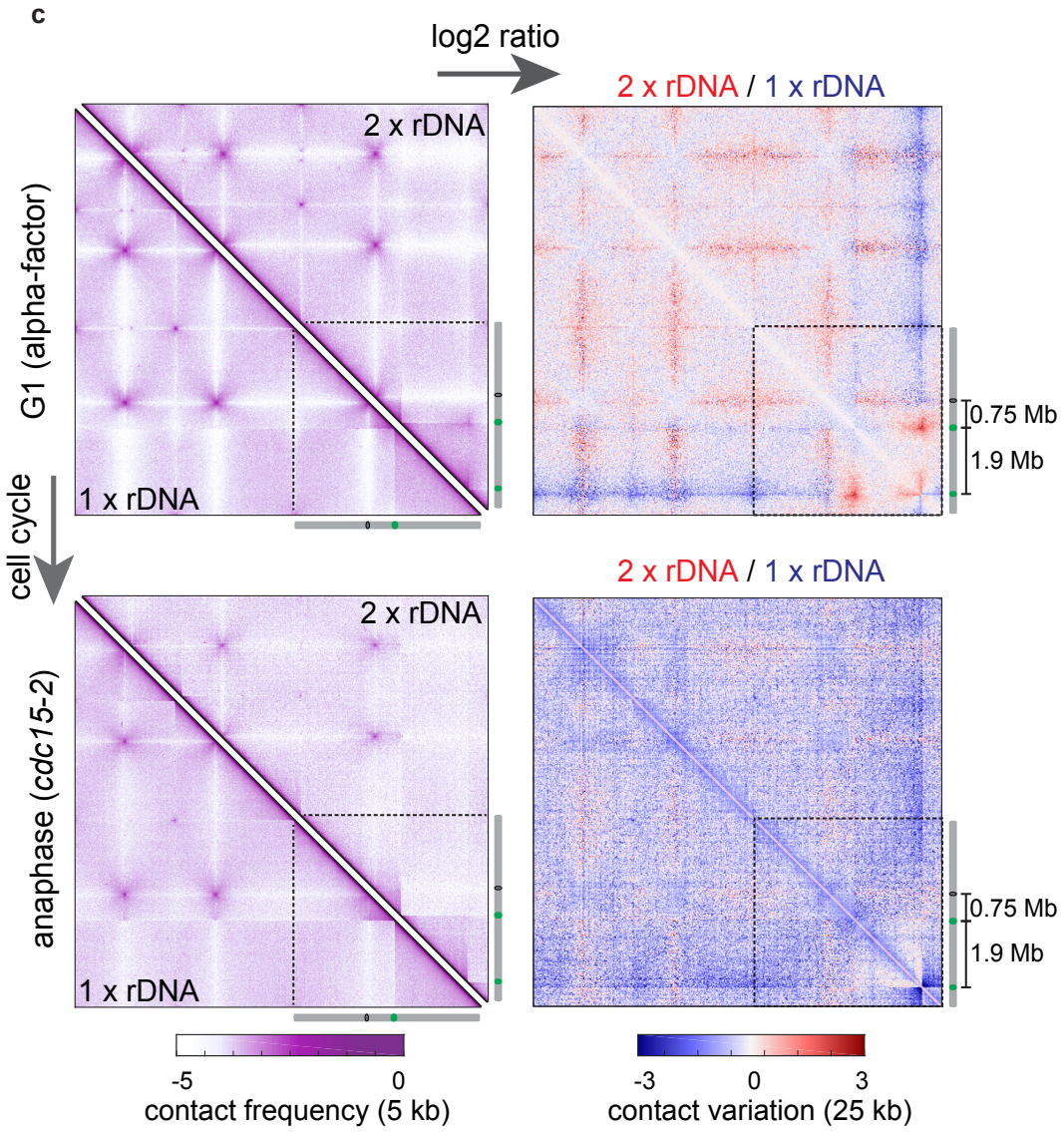
c
log2 ratio
2 x rDNA / 1 x rDNA
2 x rDNA
1 x rDNA
G1 (alpha-factor)
cell cycle
anaphase (cdc15-2)
0.75 Mb
1.9 Mb
-5
0
contact frequency (5 kb)
-3
0
3
contact variation (25 kb)

102 **Extended Data Figure 4 Cell cycle reorganization of the chromosome with twin rDNA loci**
103 **in *cis*.**
104 **a** Representative microscopy images of *n*=3 nuclei, with one or two rDNA loci, in cells
105 synchronized in G1 (alpha-factor, growth at 25ºC) and late anaphase (*cdc15-2* ts, growth at 37ºC).
106 **b** Contact probability decay *p*(*s*) in G1 vs. anaphase: shows the average decay of the
107 intrachromosomal contact frequency p between loci with respect to their genomic distance *s*. **c**
108 Left panels: Hi-C maps of megachromosomes in *n*=3, with one or two rDNA on chr *C* (dashed
109 outline), from cells synchronized in G1 (top triangle maps) and late anaphase (bottom triangle
110 maps). Right panels: contact variation (log2-ratio) of the maps shown on the left (G1: top square
111 map and anaphase: bottom square map).
112

113 **Extended Data Figure 5 Duplicated rDNA loci may lead chromosome mispairing in meiosis.**

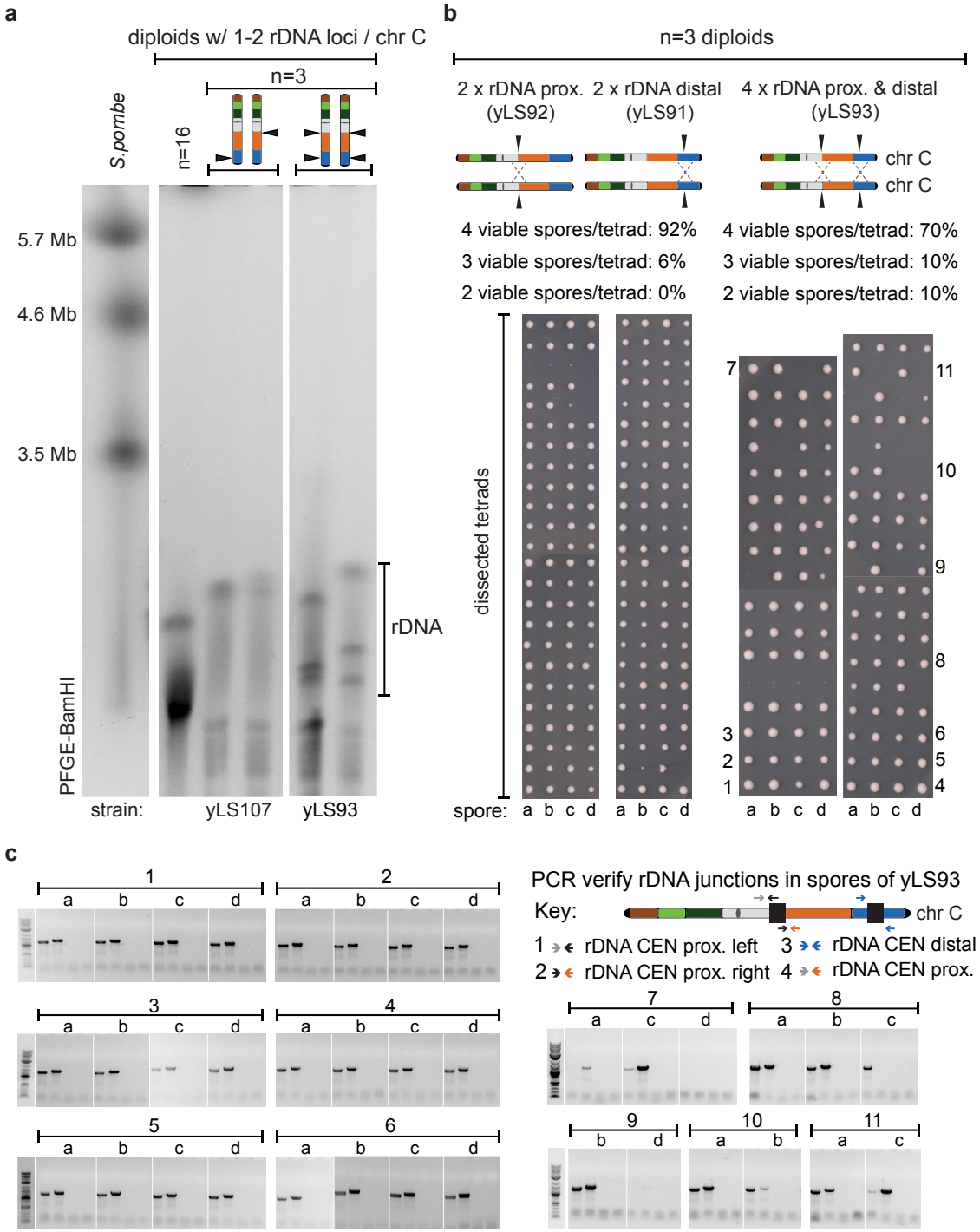

114

115 **Extended Data Figure 5 Duplicated rDNA loci may lead chromosome mispairing in meiosis.**

116 **a** PFGE and BamHI digest of diploids of *n*=16 and *n*=3 strains, with different number and position

117 of the rDNA locus. Run specifications: *S. pombe* program for mega-size chromosome separation.

118 **b** Sporulation experiments of *n*=3 diploids with single and double pairs of rDNA loci. Percentage

119 of tetrads (asci) with 2, 3 or 4 viable spores is indicated for each strain. **c** PCR verification of rDNA

120 junctions, sampling 4 different sequences in 36 spores originated from 11 different tetrads.

121